

**GREEN AND ECOFRIENDLY SYNTHESIS OF NICKEL OXIDE
NANOPARTICLES: CHARACTERIZATION AND PHOTOCATALYTIC
ACTIVITY**

KHOR HUI WEN

BACHELOR OF SCIENCE (HONS) CHEMISTRY

FACULTY OF SCIENCE

UNIVERSITI TUNKU ABDUL RAHMAN

MAY 2018

**GREEN AND ECOFRIENDLY SYNTHESIS OF NICKEL OXIDE
NANOPARTICLES: CHARACTERIZATION AND PHOTOCATALYTIC
ACTIVITY**

By

KHOR HUI WEN

A project report submitted to the Department of Chemical Science

Faculty of Science

Universiti Tunku Abdul Rahman

in partial fulfillment of the requirements for the degree of

Bachelor of Science (Hons) Chemistry

May 2018

ABSTRACT

GREEN AND ECOFRIENDLY SYNTHESIS OF NICKEL OXIDE NANOPARTICLES: CHARACTERIZATION AND PHOTOCATALYTIC ACTIVITY

KHOR HUI WEN

Nickel oxide (NiO) is a *p*-type semiconductor with a wide band gap (3.6 – 4.0 eV) and large excitation binding energy. Nowadays, there are various physical and chemical methods to synthesize NiO NPs which may be toxic and potentially dangerous to the environment and biological systems. Therefore, it is a great demand for developing a simple, low cost and environmentally-friendly green method for synthesizing of NiO NPs. In this study, NiO NPs were synthesized by using *Carica Papaya* peel extract as a reducing and stabilizing agent and nickel(II) nitrate hexahydrate as a precursor. Papaya peel extract was prepared by heating papaya peel with deionized water for 30 minutes and the extract was filtered through filter paper twice. Then, nickel(II) nitrate hexahydrate was added into the extract and the solution was heated continuously with stirring until dark green paste was formed. Upon reduction process, the colour of solution was changed from yellow to green. The dark green paste was turned into black powder of NiO

NPs upon calcination at 450 °C for 2 hours. Characteristics of synthesized NiO NPs were subsequently determined by XRD, SEM, FTIR, EDX and UV-Vis. The absorption band at 458 cm⁻¹ is corresponding to the stretching vibration of NiO are confirmed by FTIR spectrum. XRD pattern revealed that the synthesized NiO NPs were face centered cubic structure with average crystallite size of 13.39 nm. SEM showed that the synthesized NiO nanoparticles are spherical in shape with an average particle size of 66.3 nm. The photocatalytic activity of NiO NPs has been investigated by degradation of MB dye aqueous solution with exposure to sunlight. The extent of dye degradation by NiO NPs was monitored by using UV-Vis spectrophotometer. The synthesized NiO NPs have been successfully used as a photocatalyst as 93.09% MB dye was successfully degraded within 320 mins.

ABSTRAK

SINTESIS, PENCIRIAN DAN AKTIVITI FOTOKATALITIK

NIKEL OKSIDA NANOPARTIKEL

KHOR HUI WEN

Nikel oksida merupakan p-jenis semikonduktor yang terkenal dengan jurang jalur (3.6 – 4.0 eV) dan mempunyai tenaga ikatan teruja yang sangat tinggi. Pada masa kini, terdapat pelbagai kaedah fizikal dan kimia untuk mensintesis nanopartikel nikel oksida yang mungkin toksik dan berbahaya kepada alam sekitar dan sistem biologi. Oleh itu, permintaan yang besar diperlukan untuk mensintesis nanopartikel nikel oksida dengan cara yang lebih mudah, melibatkan kos rendah dan menggunakan kaedah hijau mesra alam. Dalam kajian ini, nanopartikel nikel oksida telah disintesis dengan menggunakan *Carica* ekstrak kulit betik sebagai agen penurunan dan agen penstabilan dan nikel(II) nitrat heksahidrat sebagai pelopor. Ekstrak kulit betik telah disediakan dengan memanaskan kulit betik dengan air ternyahion selama 30 minit dan ekstrak ditapis melalui kertas penapis dua kali. Kemudian, nikel(II) nitrat heksahidrat telah ditambah ke dalam ekstrak dan larutan dipanaskan secara berterusan dengan kacau sehingga pes hijau gelap terbentuk.. Dengan menjalani proses penurunan, warna penyelesaian telah

berubah dari kuning ke hijau. Pes hijau gelap telah bertukar menjadi serbuk hitam nanopartikel nikel oksida setelah kalsinasi pada 450 °C selama 2 jam. Pencirian nanopartikel nikel oksida yang disintesis dikenalpastikan dengan menggunakan XRD, SEM, FTIR, EDX dan UV-Vis spektroskopi. Jalur penyerapan pada 458 cm^{-1} bersamaan dengan getaran regangan nanopartikel nikel oksida disahkan oleh FTIR spektrum. XRD corak mendedahkan bahawa nanopartikel nikel oksida disintesis telah berpusat muka struktur padu dengan purata saiz crystallite daripada 13.39 nm. SEM menunjukkan bahawa nanopartikel nikel oksida disintesis adalah berbentuk bulat dengan saiz zarah purata 66.3 nm. Aktiviti fotokatalitik nanopartikel nikel oksida telah diperiksa dengan degradasi pewarna biru methylene dalam larutan akueus di bawah penyinaran cahaya matahari. Tahap degradasi oleh nanopartikel nikel oksida telah dipantau dengan menggunakan spektroskopi ultra lembayung-cahaya nampak. Nanopartikel nikel oksida yang disintesis telah berjaya digunakan sebagai fotokatalis kerana 93.09% pewarna biru methylene telah berjaya diturunkan dalam 320 minit.

ACKNOWLEDGEMENTS

First of all, I would like to express my sincere gratitude to Faculty of Science, Universiti Tunku Abdul Rahman (UTAR) for providing me a great chance to conduct the research for my final year project and enhancing my experience in research field.

Next, I would like to express my deep appreciation to my final year project's supervisor, Dr. Mohammad Aminuzzaman for his guidance and advices all the time in helping me to make my work easier and proficient for complete my final year project successfully. I really appreciate on his willingness to spend a lot of time to supervise me, discuss the problems faced together with me and provide the suitable solutions and teach me a lot of new knowledge as well as lab skills.

Furthermore, I want to take this opportunity to thank the lab officers, Mr Leong Thung Lim, Mr Seou Chi Kien and Mr Goh Wee Sheng for providing me a lot of useful techniques on handling instruments correctly and helping me to run analysis for my synthesized product.

Last but not least, I would like to give special thanks to my family, friends and lab partners (Ms Lee Yu Mei, Ms Ng Sook Ling and Ms Chew Ming Yi) for their endless support and encouragement throughout the progress of this research.

DECLARATION

I hereby declare that this final year project report is based on my original work except for quotations and citations which have been duly acknowledged. I also declare that it has not been previously or concurrently submitted for any other degree at UTAR or other institutions.

KHOR HUI WEN

APPROVAL SHEET

I certify that, this final year project report entitled "**GREEN AND ECOFRIENDLY SYNTHESIS OF NICKEL OXIDE NANOPARTICLES: CHARACTERIZATION AND PHOTOCATALYTIC ACTIVITY**" was prepared by KHOR HUI WEN and submitted as partial fulfillment of the requirements for the degree of Bachelor of Science (Hons) Chemistry at Universiti Tunku Abdul Rahman.

Approved by:

Date: _____

(Asst. Prof. Dr. Mohammod Aminuzzaman)

Supervisor

Department of Chemical Science

Faculty of Science

Universiti Tunku Abdul Rahman

FACULTY OF SCIENCE
UNIVERSITI TUNKU ABDUL RAHMAN

Date: _____

PERMISSION SHEET

It is hereby certified that **KHOR HUI WEN** (ID No: **14ADB02215**) has completed this thesis entitled “GREEN AND ECOFRIENDLY SYNTHESIS OF NICKEL OXIDE NANOPARTICLES: CHARACTERIZATION AND PHOTOCATALYTIC ACTIVITY” under the supervision of **ASST. PROF. DR. MOHAMMOD AMINUZZAMAN** from Department of Chemical Science, Faculty of Science.

I hereby give permission to the University to upload the softcopy of my thesis in pdf format into the UTAR Institutional Repository, which may be made accessible to the UTAR community and public.

Yours truly,

(KHOR HUI WEN)

TABLE OF CONTENTS

	Page
ABSTRACT	ii
ACKNOWLEDGEMENTS	vi
DECLARATION	vii
APPROVAL SHEET	viii
PERMISSION SHEET	ix
TABLE OF CONTENTS	x
LIST OF TABLES	xiii
LIST OF FIGURES	xiv
LIST OF ABBREVIATIONS	xviii
 CHAPTER	
1 INTRODUCTION	1
1.1 Background of Study	1
1.2 Nickel Oxide Nanoparticles	3
1.2.1 Synthesis of Nickel Oxide Nanoparticles	5
1.3 Mechanism of Photocatalysis in Degradation of Dye	14
1.4 Objectives of Study	17

2	LITERATURE REVIEW	18
2.1	Green Synthesis of Nickel Oxide Nanoparticles	18
2.1.1	Synthesis of NiO NPs by using Plant Extracts	20
2.1.2	Synthesis of NiO NPs by using Microorganisms	37
3	METHODOLOGY	40
3.1	Chemicals	40
3.2	Green Synthesis of Nickel Oxide Nanoparticles	41
3.2.1	Preparation of <i>Carica Papaya</i> Peel Extract	41
3.2.2	Synthesis Process of NiO NPs	43
3.3	Characterization of Synthesized Nickel Oxide Nanoparticles	45
3.4	Photocatalytic Activity of Synthesized Nickel Oxide Nanoparticles	50
3.4.1	Preparation of Methylene Blue (MB) Dye Aqueous Solutions	50
3.4.2	Photocatalytic Dye Degradation of Methylene Blue (MB) using synthesized NiO NPs as function of time	50
3.4.3	Determination of Percentage of Degradation	53

4	RESULTS AND DISCUSSION	54
4.1	Green Synthesis of Nickel Oxide Nanoparticles	54
4.2	Characterization of Synthesized Nickel Oxide Nanoparticles	56
4.2.1	X-ray Diffraction (XRD)	57
4.2.2	Energy Dispersive X-ray Spectroscopy (EDX)	59
4.2.3	Fourier Transform Infrared Spectroscopy (FTIR)	61
4.2.4	Ultraviolet-Visible Spectroscopy (UV-Vis)	64
4.2.5	Scanning Electron Microscope (SEM)	68
4.3	Evaluation of Photocatalytic Activity of Synthesized Nickel Oxide Nanoparticles	70
4.3.1	Degradation of Methylene Blue (MB) Dye in Aqueous Solution Using NiO NPs under Solar Irradiation	71
5	CONCLUSION	78
	REFERENCES	80
	APPENDICES	84

LIST OF TABLES

Table		Page
1.1	Conventional methods in metal oxide nanoparticles synthesis.	7
1.2	Classification of bottom-up approaches in green synthesis.	8
3.1	Time intervals during dye degradation process.	52
4.1	EDX analysis processing data.	59

LIST OF FIGURES

Figure		Page
1.1	Size of nanoparticles.	2
1.2	Applications of NiO NPs.	4
1.3	Top-down and bottom-up approaches for the synthesis of nanoparticles.	6
1.4	Mechanisms of nanoparticle synthesis.	9
1.5	Mechanism of plant mediated synthesis of metal and metal oxide nanoparticles.	11
1.6	Schematic diagram showing the mechanisms behind the biogenic synthesis of metallic nanoparticles.	12
1.7	Mechanism of microbes mediated synthesis of metal and metal oxide nanoparticles.	13
1.8	Schematic diagram of photocatalytic degradation mechanism.	14
2.1	(a) <i>Calotropis gigantea</i> plant and (b) leaf extract of <i>Calotropis gigantea</i> and biosynthesized NiO NPs.	21
2.2	(a) FESEM image, (b) TEM image and (c) EDX spectrum of biosynthesized NiO NPs.	21
2.3	(a) XRD pattern and (b) FTIR spectrum of biosynthesized NiO NPs.	22

2.4	XRD pattern of NiO NPs prepared using <i>Moringa oleifera</i> plant extract.	23
2.5	(a–i) HRTEM images of NiO NPs prepared using <i>Moringa oleifera</i> plant extract.	24
2.6	(a) EDX spectrum and (b) FTIR spectrum of NiO NPs prepared using <i>Moringa oleifera</i> plant extract.	24
2.7	(a) XRD analysis of NiO and its two different annealing temperatures, (b) FTIR analysis of NiO (i) as-prepared (ii) 350 °C and (iii) 450 °C samples and (c) EDAX analysis of NiO NPs.	26
2.8	(a) TEM and (b) SEM analysis of NiO NPs.	27
2.9	(a) EDS spectrum, (b) XRD pattern and (c) ATR-FTIR spectrum of synthesized NiO NPs.	28
2.10	HRTEM image of synthesized NiO NPs.	29
2.11	(a) FTIR spectrum and (b) XRD pattern of synthesized NiO NPs.	30
2.12	SEM images of NiO NPs.	30
2.13	TEM image of NiO NPs.	31
2.14	(a) XRD pattern and (b) IR spectrum of NiO NPs.	32
2.15	(a) TEM image and (b) SEM image of biosynthesized NiO NPs.	33
2.16	XRD pattern of biosynthesized NiO NPs.	33

2.17	(a) Absorbance spectra and (b) Tauc plot of biosynthesized NiO NPs.	34
2.18	XRD pattern of NiO NPs.	35
2.19	(a,b) HRSEM images of NiO NPs.	36
2.20	(a,b) HRTEM images of NiO NPs.	36
2.21	XRD pattern of NiO NPs (a) as prepared, (b) after annealing at 400 °C and (c) after annealing at 600 °C.	38
2.22	TEM images of annealed NiO NPs (a) at 400 °C and (b) at 600 °C.	38
2.23	FTIR spectra of annealed NiO NPs (a) at 400 °C and (b) at 600 °C.	39
3.1	Preparation of <i>Carica Papaya</i> Peel Extract.	42
3.2	Synthesis of NiO NPs using <i>Carica Papaya</i> Peel Extract.	44
3.3	Shimadzu XRD 6000.	46
3.4	Perkin Elmer Spectrum RX1 Fourier Transform Infrared Spectrometer.	47
3.5	UV-Vis Single Beam Spectrophotometer (Thermo Fischer Scientific Genesys 10S Series UV- Visible Spectrophotometer).	48
3.6	Scanning Electron Microscope (JEOL JSM-6701F).	49
3.7	Energy Dispersive X-Ray Diffractometer.	49

3.8	Photocatalytic activity of synthesized NiO NPs under solar irradiation.	53
4.1	Photograph of NiO NPs synthesized using <i>Carica Papaya</i> peel extract.	55
4.2	XRD pattern of synthesized NiO NPs.	57
4.3	EDX spectrum of synthesized NiO NPs.	59
4.4	FTIR comparative spectra of synthesized NiO NPs and papaya peel extract.	61
4.5	UV-Visible spectrum of synthesized NiO NPs.	64
4.6	Tauc plot of synthesized NiO NPs.	66
4.7	SEM images of synthesized NiO NPs at different magnifications, X = 15000, 20000 and 30000.	68
4.8	Chemical structure of MB.	71
4.9	UV-Vis spectra of MB dye degradation in the presence of photocatalyst NiO NPs under solar irradiation as a function of contact time (minutes).	72
4.10	Photograph of color change of degraded MB dye aqueous solution at different time interval.	72
4.11	Percentage of degradation of MB dye solution as a function of time.	73
4.12	Photocatalytic reaction pathway of MB dye.	75
4.13	Graph of C/C_0 against time.	76

LIST OF ABBREVIATIONS

A	Ampere or absorbance
Å	Angstrom
A ₀	Initial absorbance of dye solution
A _t	Absorbance of dye solution at a given contact time
ATR-FTIR	Attenuated Total Reflection-Fourier Transform Infrared
BET	Brunauer-Emmett-Teller
C	Carbon
c	Speed of light
CB	Conduction band
cm ⁻¹	Frequency unit or wavenumber
CO ₂	Carbon dioxide
Cu	Copper
D	Average crystalline diameter size
E _{bg}	Band gap energy
EDS/EDX	Energy Dispersive X-ray Spectroscopy
eV	Electronvolt
e ⁻	Electron
FESEM	Field Emission Scanning Electron Microscopy
FTIR	Fourier Transform Infrared Spectroscopy
FWHM	Full width half maximum

g	Gram
GC-MS	Gas chromatography-mass spectrometry
h	Planck's constant
h^+	Hole
$h\nu$	Light
H ₂ O	Water molecule
H ₂ O ₂	Hydrogen peroxide
HRSEM	High Resolution Scanning Electron Microscope
HRTEM	High Resolution Transmission Electron Microscopy
JCPDS	Joint Committee Powder Diffraction Standards
k	Scherrer constant
KBr	Potassium bromide
kV	Kilovolt
L	Liter
LC-MS	Liquid chromatography-mass spectrometry
M	Mega or molar concentration
m	Milli
MB	Methylene Blue
MS	Mass spectrum
Ni	Nickel
NiO	Nickel(II) oxide
NiO NPs	Nickel oxide nanoparticles
Ni(0)	Nickel(0)

Ni(II)	Nickel(II)
nm	Nanometer
O	Oxygen element
O ₂	Oxygen molecule
O ₂ ⁻	Superoxide anion
OH ⁻	Hydroxide ion
·OH	Hydroxyl radical
P	Phosphorus element
PL	Photoluminescence Spectroscopy
ppm	Part per million
rpm	Revolution per minute
SEM	Scanning Electron Microscope
TEM	Transmission Electron Microscope
UV	Ultraviolet
UV-Vis	Ultraviolet-Visible
VB	Valence band
VOC	Volatile organic compounds
VSM	Vibrating sample magnetometry
W	Waltz
XPS	X-ray Photoelectron Spectroscopy
XRD	X-ray Diffraction
λ	Wavelength of X-ray source or lambda
λ _{max}	Lambda maximum

$^{\circ}\text{C}$	Degree Celsius
θ	Bragg's diffraction angle
β	Full width at half-maximum of the diffraction peak
π	Pi
μ	Micro
α	Absorption coefficient
ν	Frequency

CHAPTER 1

INTRODUCTION

1.1 Background of Study

Nanotechnology is an application based technology which applied in various fields, such as biology, chemistry, physics, biotechnology, material sciences, engineering, medicine, drug delivery, optics and food industry (Ahmed and Ikram, 2015). The uses of nanotechnology and biotechnology in biosynthesis of nanoparticles have been rapidly growing and received a considerable amount of attention for the purpose of manufacturing materials at the nano-scaled level in order to develop environmentally benign technologies (Mude et al., 2009). Nanoparticles are made up by the combination of large atoms and molecules with a size range of 1 – 100 nm. There is a great interest in synthesis of nanoparticles due to their porosity, extremely small crystal size, high chemical stability, large surface area to volume ratio and they exhibited unique properties in their application compared to the bulk materials (Akhtar, Panwar and Yun, 2013). The properties of metal oxide nanoparticles vary according to their size, shape and morphology. Nanoparticles able to provide suitable solutions to the technological and environmental problems like wastewater treatment by removal of pathogens from wastewater (Jain and Mehata, 2017).

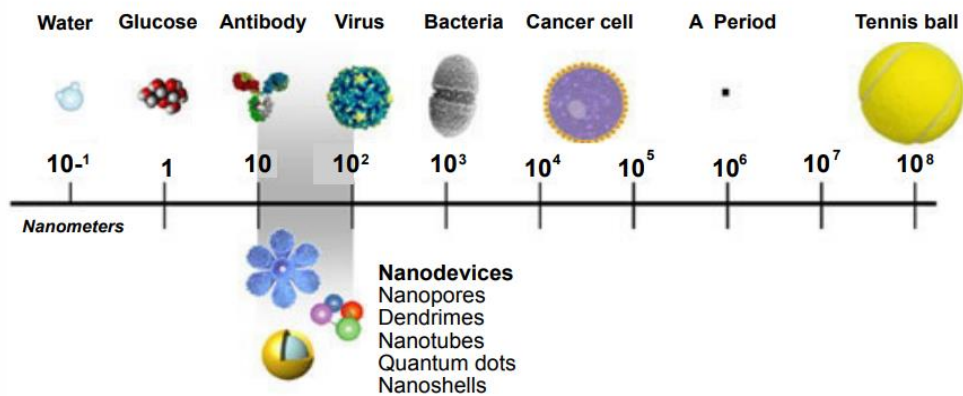


Figure 1.1 Size of nanoparticles (Chakraborty, Roy and Mondal, 2016).

1.2 Nickel Oxide Nanoparticles

Nickel oxide (NiO) is classified as one of the most common used metal oxide and have drawn a lot of interest as it provide superior properties with a wide range of potential applications in various areas such as catalysis, solar cells, semiconductors, antiferromagnetic layers gas sensors, *p*-type transparent conducting oxides, battery electrodes, magnetic materials, adsorbents, electrochemical supercapacitors, magnetic resonance imaging, electrochromic films, memory storage devices, drug delivery, water electrolysis and very recently in the treatment of cancer cells (Qing et al., 2015). They were used as an inexpensive and non-hazardous catalyst in order to enhance the reactivity and selectivity of various organic reactions including reduction of aldehydes and ketones, hydrogenation of olefins, α -alkylation of methyl ketone and inorganic reactions like decomposition of ammonia (Imran Din and Rani, 2016).

Nickel oxide nanoparticles (NiO NPs) exhibit thermal, electronic, optical, mechanical, chemical, physical, biological and magnetic properties that are significantly different than those of bulk NiO particles because of the quantum size and surface effects (El-Debaiky, El-Badry and El-Shahawy, 2017). It is a transparent *p*-type semiconductor metal oxide with wide band gap energy covering the range from 3.6 to 4.0 eV depending upon the nature of defects and their density (Imran Din and Rani, 2016). The band gap energy is the energy differences between valence band and conduction band, which means the amount

of energy required for the electrons at valence band to be excited to the conduction band under solar irradiation. The band gap energy increases as the size of the nanoparticles decreases.

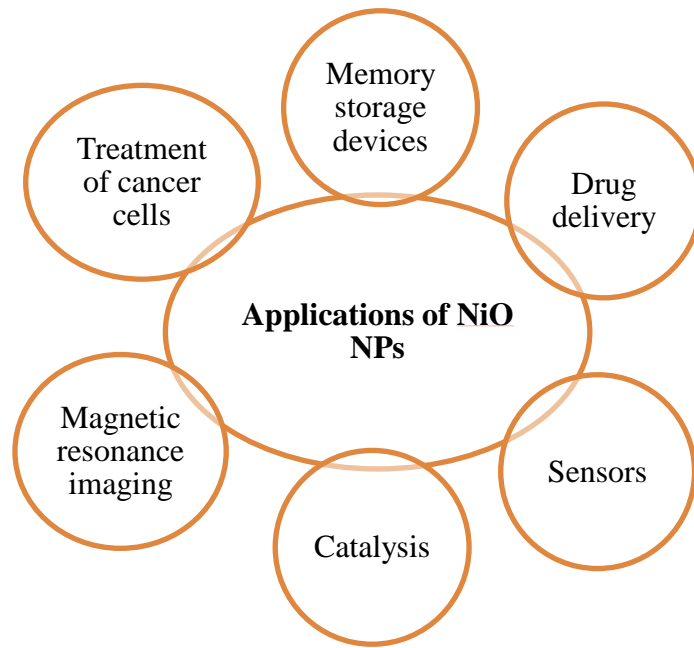


Figure 1.2 Applications of NiO NPs (Qing et al., 2015).

1.2.1 Synthesis of Nickel Oxide Nanoparticles

NiO NPs can be synthesized through various conventional techniques which includes chemical precipitation, thermal decomposition, solvothermal reduction, sol-gel, hydrothermal synthesis, ion sputtering, spray pyrolysis, co-precipitation methods, water-in-oil microemulsions and water electrolysis (Soofivand and Salavati-Niasari, 2017). Although NiO NPs usually can be successfully synthesized by physical and chemical methods in large quantities with specific shape and size for short periods of time, however, these methods have many disadvantages like extremely high cost, high energy consumption, longer reaction time, environmentally unfriendly, flammable, low production rate and involve the use of hazardous organic chemicals (Imran Din and Rani, 2016). There is a growing need to develop environmentally benign technologies in terms of alternative eco-friendly, rapid, simple operational, low cost, single step methods for synthesis of NiO NPs (Mude et al., 2009).

There are two types of common conventional methods to synthesize nanoparticles which are bottom-up (construction) approach and top-down (destruction) approach as shown in Figure 1.3 and Table 1.1. In bottom-up synthesis, the nanoparticles are built by joining atoms, molecules and smaller particles together. The nanostructured building blocks of the nanoparticles are formed at first in the bottom-up method and then the smaller particles are assembled to produce the final particle. This method mostly relies on chemical and biological methods of production (Mittal, Chisti and Banerjee, 2013).

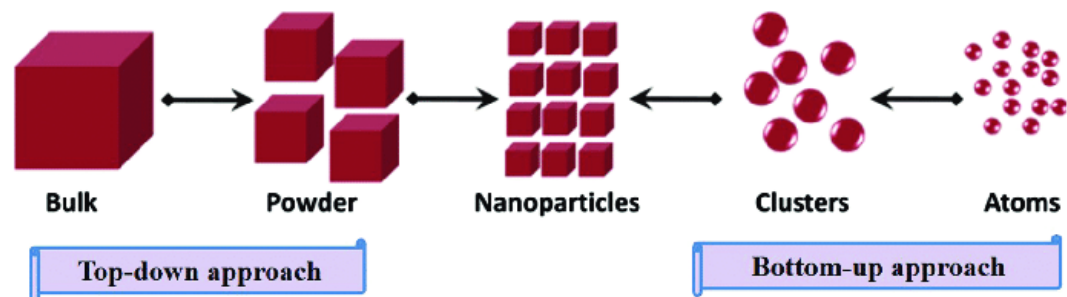


Figure 1.3 Top-down and bottom-up approaches for the synthesis of nanoparticles (Pareek et al., 2017).

In top-down synthesis, nanoparticles are produced by the reduction in size from the starting materials which is able to achieve by various physical and chemical treatments. There is a major limitation when using this method as top-down production methods introduce imperfections in the surface structure of the nanoparticles and the surface chemistry and the other physical properties of nanoparticles are highly dependent on the surface structure (Mittal, Chisti and Banerjee, 2013).

Table 1.1 Conventional methods in metal oxide nanoparticles synthesis

(Haleemkhan, Naseem and Vardhini, 2015).

Bottom-Up Methods (construction)	Top-Down Methods (destruction)
Supercritical fluid synthesis	Mechanical/Ball milling
Chemical/electrochemical precipitation	Chemical etching
Use of templates	Sputtering
Plasma or flame spraying synthesis	Thermal/Laser ablation
Sol-gel process	Explosion process
Laser pyrolysis	Microwave
Aerosol based process	Ultra films
Chemical vapor deposition (CVD)	Plasma arching
Atomic/molecular condensation	Lithography

Green synthesis is one kind of bottom-up methods. There are two types of classifications in bottom-up approaches for green synthesis which are microscopic and macroscopic as shown in Table 1.2.

Table 1.2 Classification of bottom-up approaches in green synthesis (Haleemkhan, Naseem and Vardhini, 2015).

Bottom-Up Methods (Green Synthesis)	
Microscopic	Macroscopic
<ul style="list-style-type: none"> ▪ Bacteria ▪ Actinomycetes ▪ Fungi 	<ul style="list-style-type: none"> ▪ Algae ▪ Sea weeds ▪ Plant extracts (leaves, bark, stem, shoots, seeds, latex, secondary metabolites, roots, twigs, peel, fruit, seedlings, essential oils, tissue cultures, gum)

The biosynthetic methods by employing the uses of leaf extract, plant extract, fruit peel extract, bacteria, fungus and enzymes as an environmentally benign materials in the synthesis of nanoparticles process have been considered as a green route and often attributed to numerous advantages as it is simple, environment friendly, cost effective, low pressure, readily scalable, less energy required, low temperature, easily scaled up for large scale synthesis, safe to handle and free from toxic chemicals being used for the nanoparticles synthesis process (Jain et al., 2009). Therefore, green synthesis of NiO NPs is preferable

compared to the physical and chemical methods which having significant negative impact on environment. The plant based and fruit based materials are suitable in large-scale biosynthesis of nanoparticles. This is due to the presence of bioactive compounds like polyphenols, proteins, alkaloids, phenolic compounds, flavonoids, cofactors, terpenoids, polysaccharides and flavones compounds to be act as reducing agent, stabilizing agent and capping agent and thus resulting in more stable with a better defined size and morphology of nanoparticles than those produced by the conventional methods (Sharma et al., 2015). These biomolecules components are responsible for converting metal ions into metal nanoparticles by reduction mechanism. The mechanism for synthesis of nanoparticles is shown in Figure 1.4.

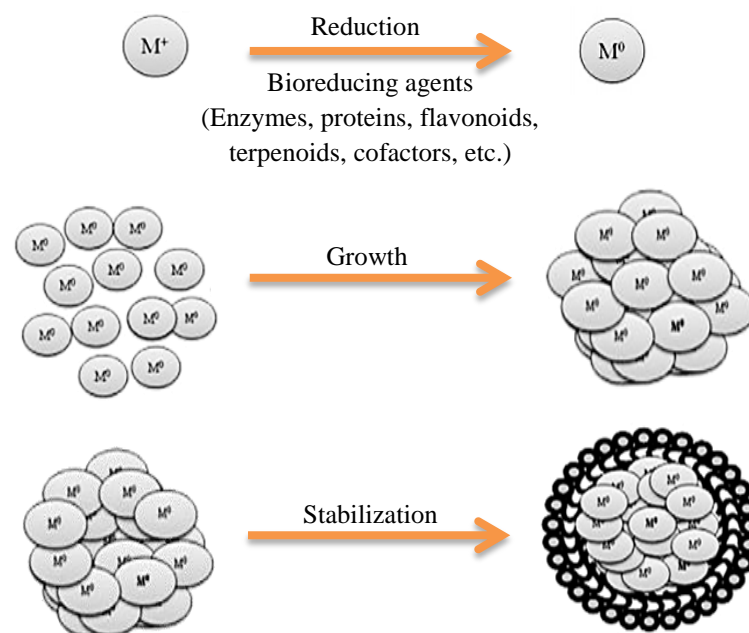


Figure 1.4 Mechanisms of nanoparticle synthesis (Mittal, Chisti and Banerjee, 2013).

Electronic density on the conjugate salts of metal increases results from the reduction of metal ions into metal atoms by using biomolecules components and also the metal salts have high reduction potential due to their tendency to donate electrons. Therefore, metals able to be reduced into their stable form (zero-valent states) by using leaf extract, plant extract, fruit peel extract, bacteria, fungus and enzymes as the metals in ionic form can easily get detached from anionic form. Plants have limited competency in reduction of metal ions which depends on the reduction potential of metal species (Akhtar, Panwar and Yun, 2013). Mostly the hydroxyl groups present in flavonoids (such as quercetin) and polyphenols is responsible to act as a role of reducing agent for plant mediated synthesis while the donation of electrons by reductase enzyme of bacterial or fungal cell wall is responsible to reduce the metal ions into metal nanoparticles for microbial mediated synthesis (Imran Din and Rani, 2016).

In the mechanism of plant mediated synthesis, there are mainly three phases: (1) activation phase which involves reduction of metal ions and nucleation of reduced metal atoms; (2) growth phase which involves the clustering of small nanoparticles to form larger size nanoparticles and subsequently growth of nanoparticles by further reduction of metal ions; (3) termination phase which decides the final shape of nanoparticles (Imran Din and Rani, 2016). The factors like pH, concentration and nature of reducing agent used affect the features of each stage (Jain and Mehata, 2017). The metal atoms are then air-dried or calcined in air in order to obtain the final metal oxide nanoparticles (Imran Din

and Rani, 2016). The schematic diagrams for mechanism of plant mediated synthesis are shown in Figure 1.5 and Figure 1.6.

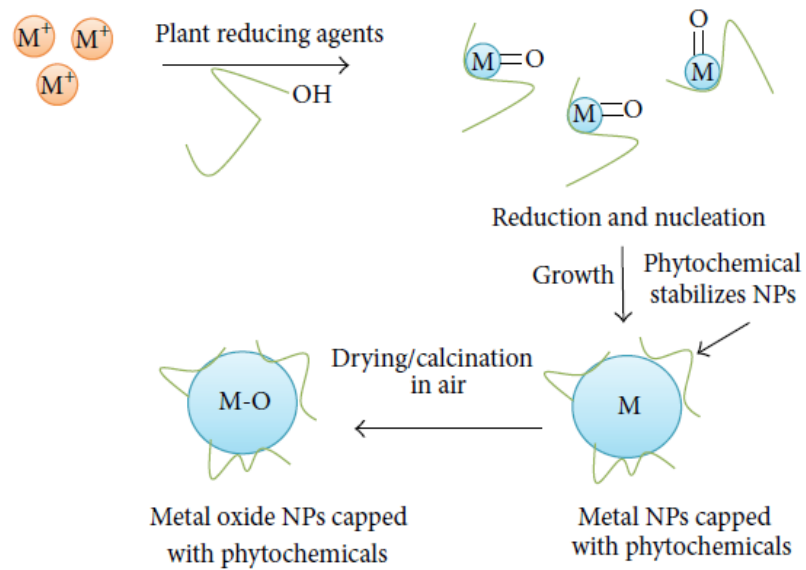


Figure 1.5 Mechanism of plant mediated synthesis of metal and metal oxide nanoparticles (Imran Din and Rani, 2016).

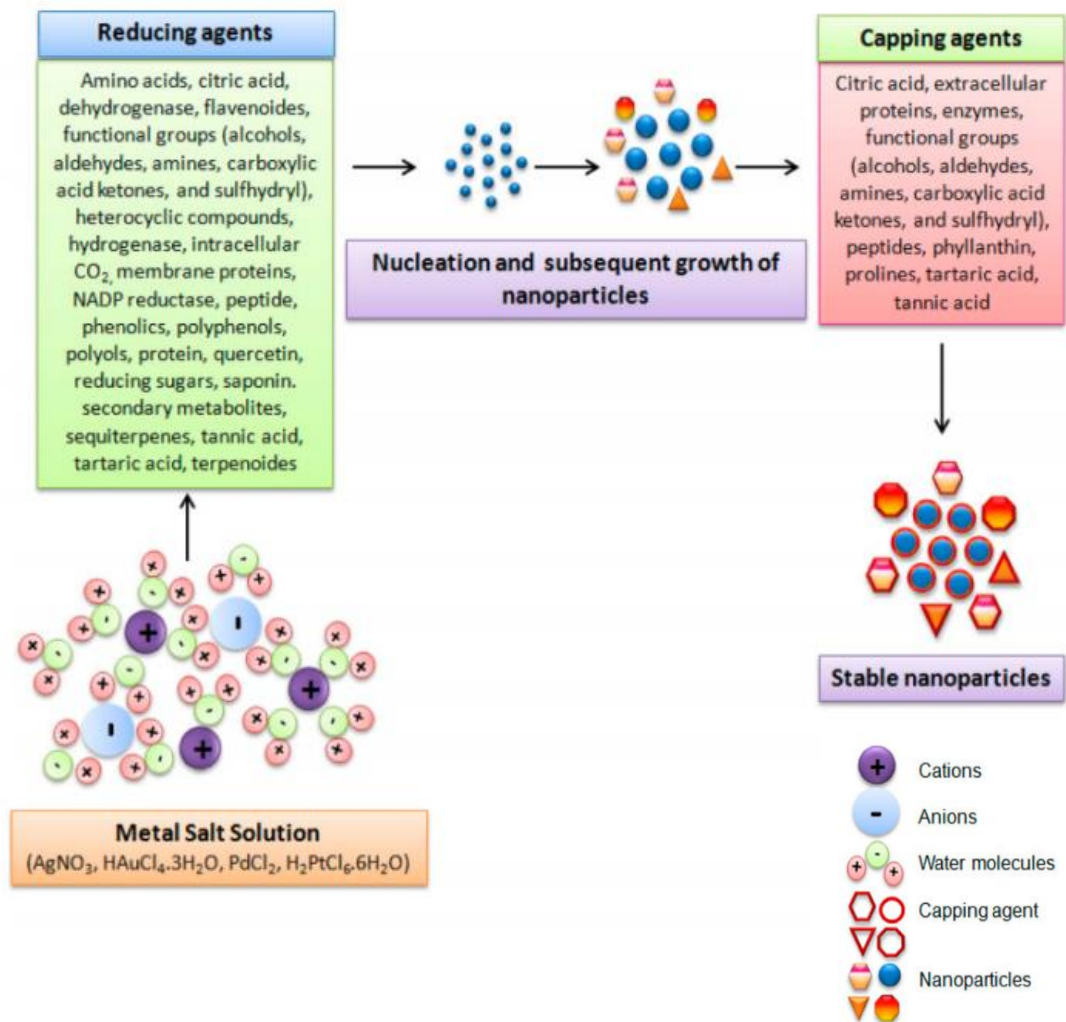


Figure 1.6 Schematic diagram showing the mechanisms behind the biogenic synthesis of metallic nanoparticles (Akhtar, Panwar and Yun, 2013).

In the mechanism of microbial mediated synthesis, there are mainly three phases: (1) metal cations are trapped by cell wall of bacterial or fungal due to electrostatic interaction between positively charged metal cation and negatively charged cell wall; (2) reductase enzyme is then released by cell wall to reduce metal ions into metal atom; (3) aggregation of these atoms to form metal nanoparticles. The

biomolecules of bacterium or fungal help to prevent further aggregation of metal nanoparticles by capping the formed nanoparticles and eventually the formed metal nanoparticles will be diffused out from cell wall. The metal atoms are then air-dried or calcined in air in order to obtain the final metal oxide nanoparticles (Imran Din and Rani, 2016). The schematic diagram for mechanism of microbial mediated synthesis is shown in Figure 1.7.

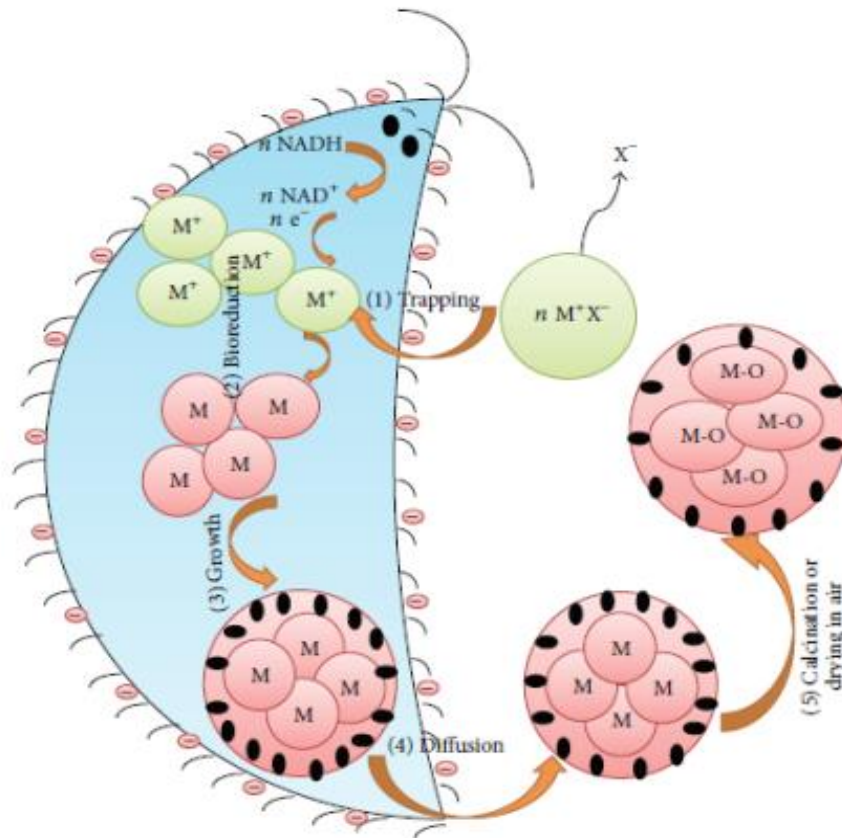


Figure 1.7 Mechanism of microbes mediated synthesis of metal and metal oxide nanoparticles (Imran Din and Rani, 2016).

1.3 Mechanism of Photocatalysis in Degradation of Dye

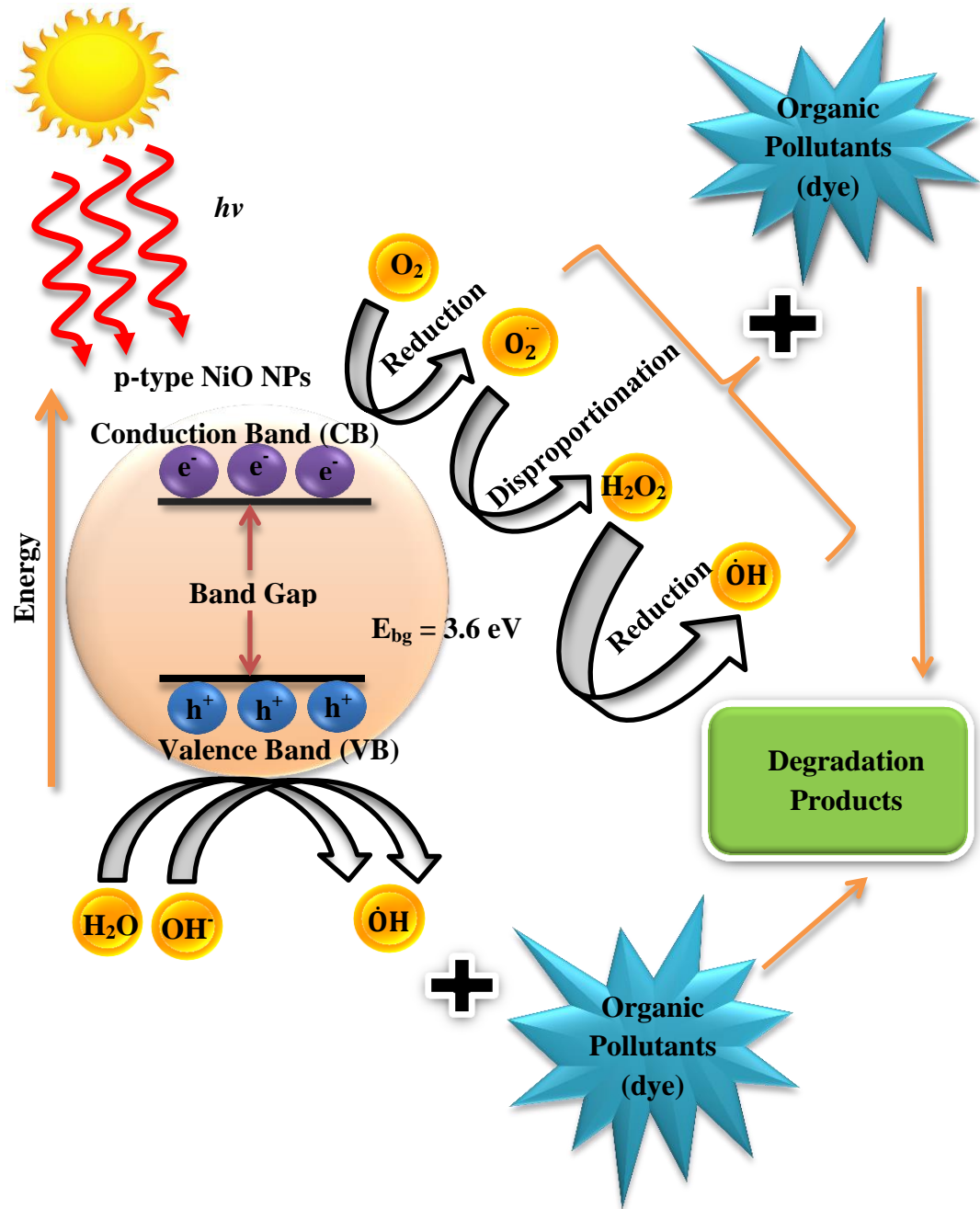
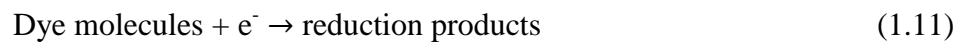
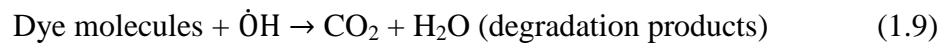
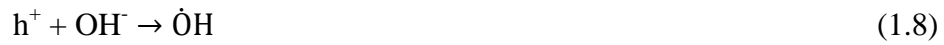


Figure 1.8 Schematic diagram of photocatalytic degradation mechanism

(Ezhilarasi et al., 2016).

Figure 1.8 shows the photocatalytic degradation mechanism where a series of reaction occurred on the surface of NiO NPs under solar irradiation. Photocatalytic reaction is initiated when a NiO semiconductor molecule absorbs the incident photons which energy is equal or greater than that of the band gap energy and in turn causes the photo-excitation takes place to promote electrons (e^-) from valence band (VB) to conduction band (CB). This leads to the generation of holes (h^+) at the valence band and electrons (e^-) at the conduction band. These electron-hole pairs can either recombine or can interact separately with other molecules. The photo-generated holes and excited electrons possess high oxidizing and reducing properties. The photo-generated electrons react with acceptor, the molecular oxygen adsorbed on NiO NPs surface to form a series of reactive oxygen species like superoxide anion (O_2^-), hydrogen peroxide (H_2O_2) and hydroxyl radicals ($\dot{O}H$). This is so called the photo-oxidation reaction. The photo-generated holes react with electron donors, the water molecules and hydroxyl ions to form active hydroxyl radicals ($\dot{O}H$). This is so called the photo-reduction reaction (Ezhilarasi et al., 2016). The hydroxyl radicals are strong and dominant oxidizing agent which are responsible in destruction of organic pollutants dye solutions to yield almost complete mineralization of dye molecules into carbon dioxide (CO_2), water (H_2O) and relevant inorganic ions (Ajoudanian and Nezamzadeh-Ejhieh, 2015). The important reactions for degradation of organic dyes are as shown in the equations below:



Positive holes = oxidizing agent

Negative electrons = reducing agent

1.4 Objectives of Study

1. To synthesize NiO NPs through green synthetic pathway using aqueous extract of *Carica Papaya* peels.
2. To characterize NiO NPs using UV-Visible Spectroscopy (UV-Vis), Fourier Transform Infrared Spectroscopy (FTIR), Energy Dispersive X-ray Spectroscopy (EDX), X-ray Diffraction (XRD) and Scanning Electron Microscopy (SEM).
3. To evaluate the photocatalytic activity of biosynthesized NiO NPs using Methylene Blue (MB) dye solution under solar irradiation and degradation process was monitored by UV-Visible Spectroscopy (UV-Vis).

CHAPTER 2

LITERATURE REVIEW

2.1 Green Synthesis of Nickel Oxide Nanoparticles

In this literature review, NiO NPs are found to be synthesized using plant extract (*Calotropis gigantea*, *Moringa Oleifera*, neem leaves, *Agathosma betulina*, Arabic gum, *Tamarix serotina*, *Psidium guajava* and *Coriandrum sativum*) and microorganisms (*Fusarium verticillioides*) by other researchers.

Plant extracts are far more advantageous as they consist of the biomolecules which can act as a reducing agent, stabilizing agent as well as the capping agent in the synthesis of NiO NPs. The reducing agents involved in the plant extracts include the various water soluble plant metabolites (e.g. enzymes, polyphenols, proteins, alkaloids, phenolic compounds, flavonoids, cofactors, terpenoids, polysaccharides, flavones compounds, etc.) and co-enzymes that can be used to reduce metal ions to nanoparticles in a single-step green synthesis process. This reduction process is performed quite rapid, simple, easily scaled up and readily conducted at room temperature and pressure. Synthesis of NiO NPs by plant extracts is environmentally benign and economically feasible. The processes for making NiO NPs using plant extracts are readily scalable and may be less

expensive. There are diverse ranges of the plant extract are successfully used to synthesis NiO NPs. The characteristics of the synthesized NiO NPs will be influenced by the source of the plant extracts. This is due to the reason that different plant extracts contain different combinations of organic reducing agents and concentrations (Mittal, Chisti and Banerjee, 2013).

Microorganisms such as bacteria, fungi and yeast also act as the stabilizing agent and reducing agent in the synthesis of NiO NPs. The synthesis process of NiO NPs by using microorganisms offer certain advantages like easy processing, eco-friendly, economic viability, biomass handling and simple scaling up although their rate of production for NiO NPs is slower than that of the synthesis process by using plant extracts. However, synthesis of NiO NPs by using plant extract as reducing agent is more beneficial as compared to the synthesis of NiO NPs by using microorganisms extract as reducing agent because of the rapid rate of production of NiO NPs with former green reducing agent (Imran Din and Rani, 2016).

2.1.1 Synthesis of NiO NPs by using Plant Extracts

According to Sharma et al., (2015), NiO NPs were synthesized by using leaf extract of plant *Calotropis gigantea* as shown in Figure 2.1. The synthesized NiO NPs were characterized by XRD, SEM, TEM and EDX. Leaf extract of *Calotropis gigantea* consist abundance amount of proteins, polyphenols, alkaloids and flavonoids which act as active ingredients to reduce the nickel ions to nickel nanoparticles. This reduction process can be performed due to the polyphenols of the leaf extract have an easy electron loosing capacity which causes the formation of nickel-phenolate complex. The obtained complex on calcination at 400 °C produces NiO NPs. From FE-SEM analysis shown in Figure 2.2 (a), it showed that the biosynthesized NiO NPs are homogeneous, spherical and uniformly distributed with average particle sizes of 20 – 50 nm. TEM micrograph (as shown in Figure 2.2 (b)) also revealed that the biosynthesized NiO NPs consists of the aggregated spherical shape with a diameter of 20 – 50 nm. There are majorly visible peaks of Ni and O shown in the EDX spectrum in Figure 2.2 (c) which indicates the presence of Ni and O elements in the biosynthesized NiO NPs. The average particle size of biosynthesized NiO NPs determined from the XRD pattern as shown in Figure 2.3 (a) was ~ 20 nm according to Debye-Scherrer equation. From the FTIR spectrum shown in Figure 2.3 (b), the Ni-O stretching vibration appeared at the absorption band of 454 cm⁻¹ and 686 cm⁻¹. The authors reported that biosynthesized NiO NPs able to act as a good catalyst for thermal

decomposition of ammonium perchlorate and burning rate of composite solid propellants.

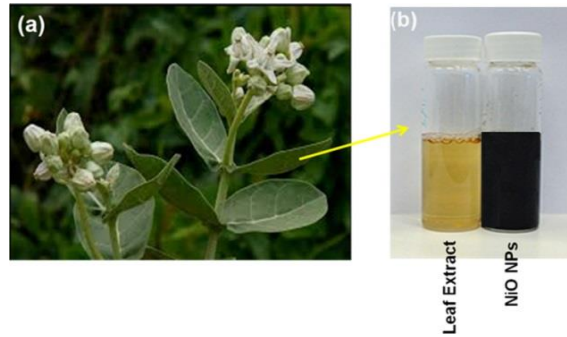


Figure 2.1 (a) *Calotropis gigantea* plant and (b) leaf extract of *Calotropis gigantea* and biosynthesized NiO NPs (Sharma et al., 2015).

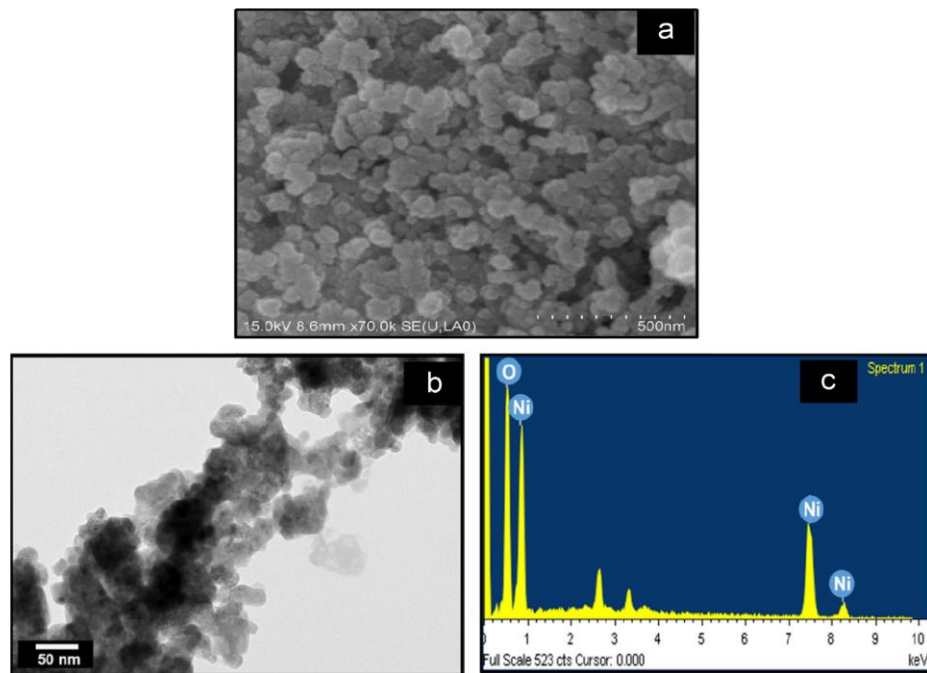


Figure 2.2 (a) FESEM image, (b) TEM image and (c) EDX spectrum of biosynthesized NiO NPs (Sharma et al., 2015).

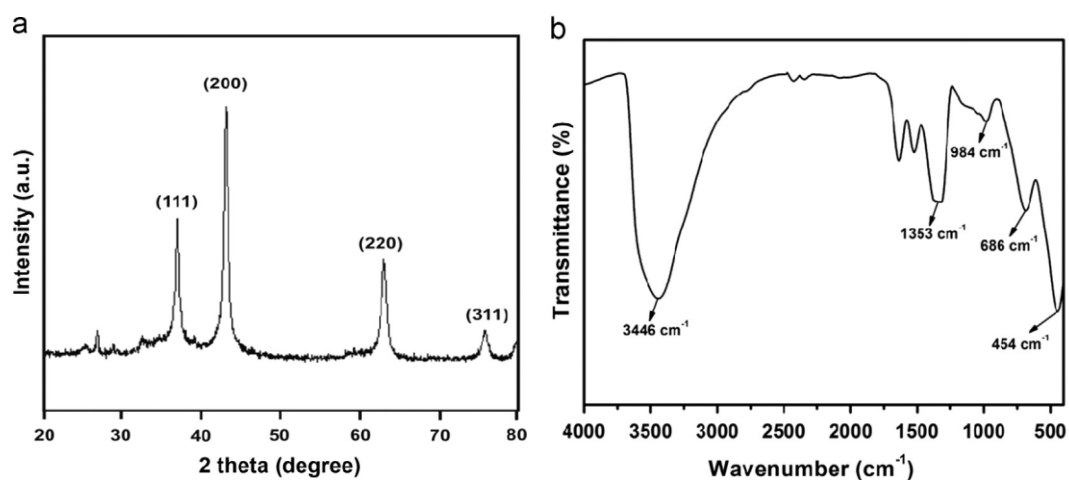


Figure 2.3 (a) XRD pattern and (b) FTIR spectrum of biosynthesized NiO NPs (Sharma et al., 2015).

Ezhilarasi et al., (2016) reported the uses of *Moringa Oleifera* plant extract to synthesize NiO NPs. The synthesized NiO NPs were characterized by XRD, FTIR, HRTEM, EDX and PL. The plant extract contains various nutrients, fatty acids, amino acids, phenolics and vitamins which can be used to capture the metal ion. The XRD pattern shown in Figure 2.4 clearly indicated the synthesized NiO NPs are highly crystalline as there are presences of strong intense and sharp peaks with crystallite size of 9.69 nm. It also showed that NiO NPs having face centered cubic phase. Besides, NiO NPs have two intense photoluminescence emissions at 305.46 nm and 410 nm. The HRTEM image shown in Figure 2.5 (a-i) revealed that the NiO NPs were small in size with slightly agglomeration and nearly spherical in shape. There are Ni and O peaks presented in the EDX spectrum as shown in Figure 2.6 (a). The stretching frequency of 965 cm⁻¹ represented the Ni-

O stretching vibration as shown in the FTIR spectrum in Figure 2.6 (b). The authors reported that NiO NPs prepared from green synthetic process shows better cytotoxicity and antibacterial activity. The unique properties of NiO NPs such as adsorbing ability, surface area and metal ion releasing enable it possess efficient cytotoxic activity against human cancer cells. Moreover, the potential of inducing oxidative stress and also the tendency to release Ni^{2+} ions inside the cell enable the NiO NPs exhibit effective antibacterial properties against bacterial pathogens.

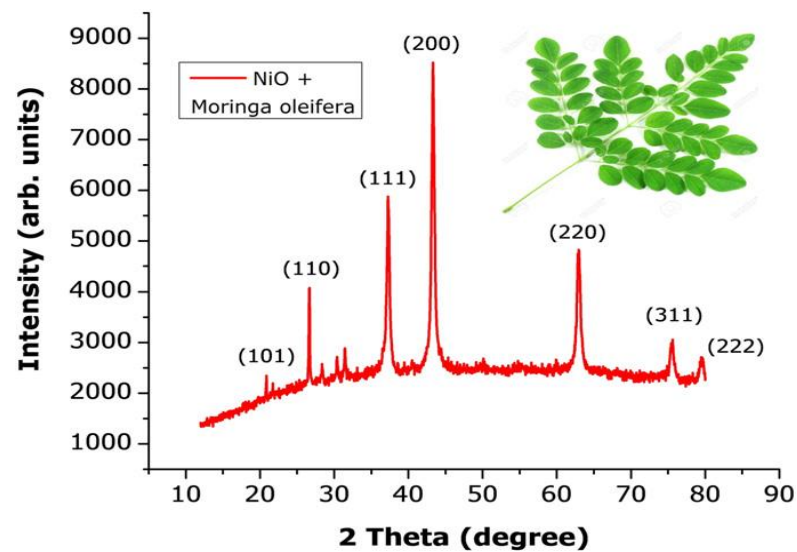


Figure 2.4 XRD pattern of NiO NPs prepared using *Moringa oleifera* plant extract (Ezhilarasi et al., 2016).

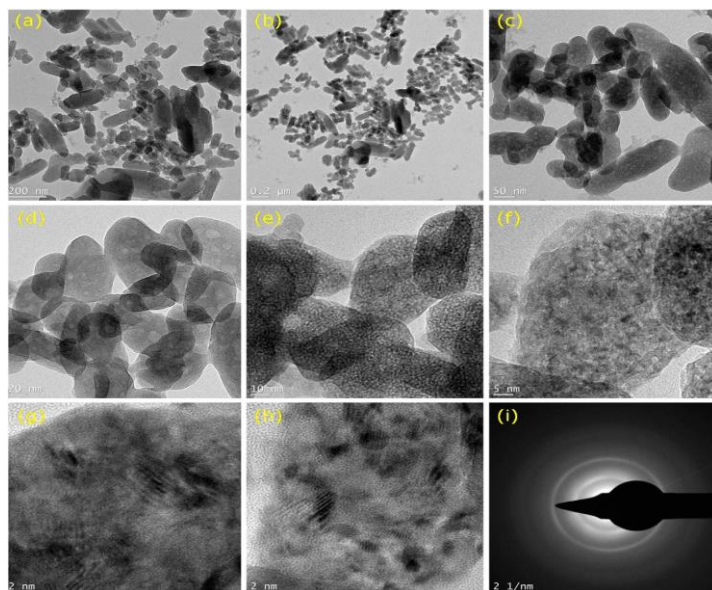


Figure 2.5 (a–i) HRTEM images of NiO NPs prepared using *Moringa oleifera* plant extract (Ezhilarasi et al., 2016).

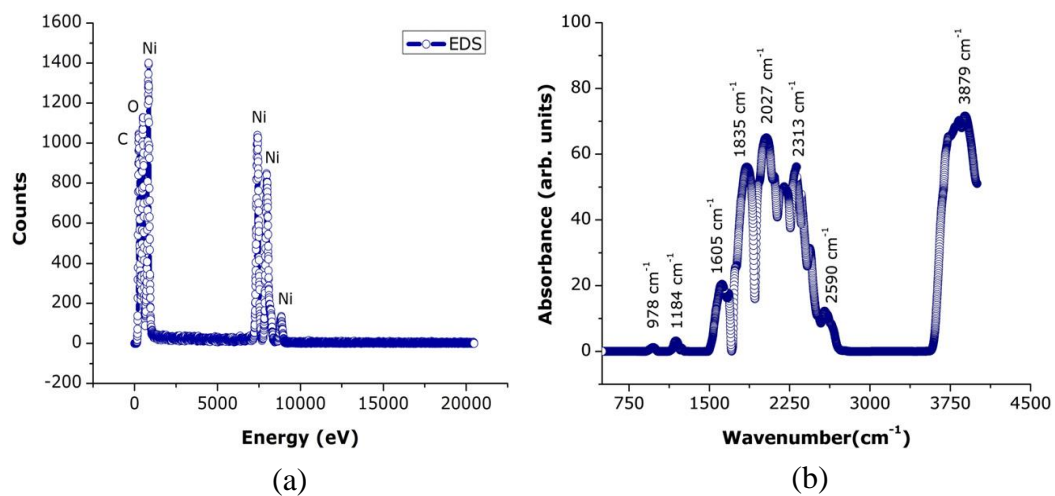


Figure 2.6 (a) EDX spectrum and (b) FTIR spectrum of NiO NPs prepared using *Moringa oleifera* plant extract (Ezhilarasi et al., 2016).

The green biosynthesis of NiO NPs by using neem leaves was reported by Helan et al., (2016). The synthesized NiO NPs were characterized by XRD, FTIR, SEM/EDAX and TEM. The leave extract able to convert metal into metal nano form by reduction mechanism as it contains various compounds with different kind of functional groups. From the XRD pattern shown in Figure 2.7 (a), there is presence of polycrystalline nature of NiO NPs (0 1 0), (0 1 1) and (0 1 2) with hexagonal crystal phase. The FTIR spectrum in Figure 2.7 (b) showed that the Ni-O stretching vibration mode occurred at the strong absorption band of 1116 cm^{-1} , 3686 cm^{-1} and 2358 cm^{-1} . The quantity of Ni and O confirmed by the EDAX spectrum shown in the Figure 2.7 (c) were 51 % and 49 % respectively and this indicated that the presence of NiO phase without any other impurity. The biosynthesized NiO NPs were in nano form with oblong shape and average particle size of $10 \pm 2\text{ nm}$ which revealed by TEM image shown in Figure 2.8 (a). The NiO NPs were in fine spherical shape with agglomerated structure as shown in SEM image in Figure 2.8 (b). The mass magnetization values determined for NiO NPs was 61 emu/g while the coercivity values for NiO NPs obtained was in the range of $0.2 - 0.4$.

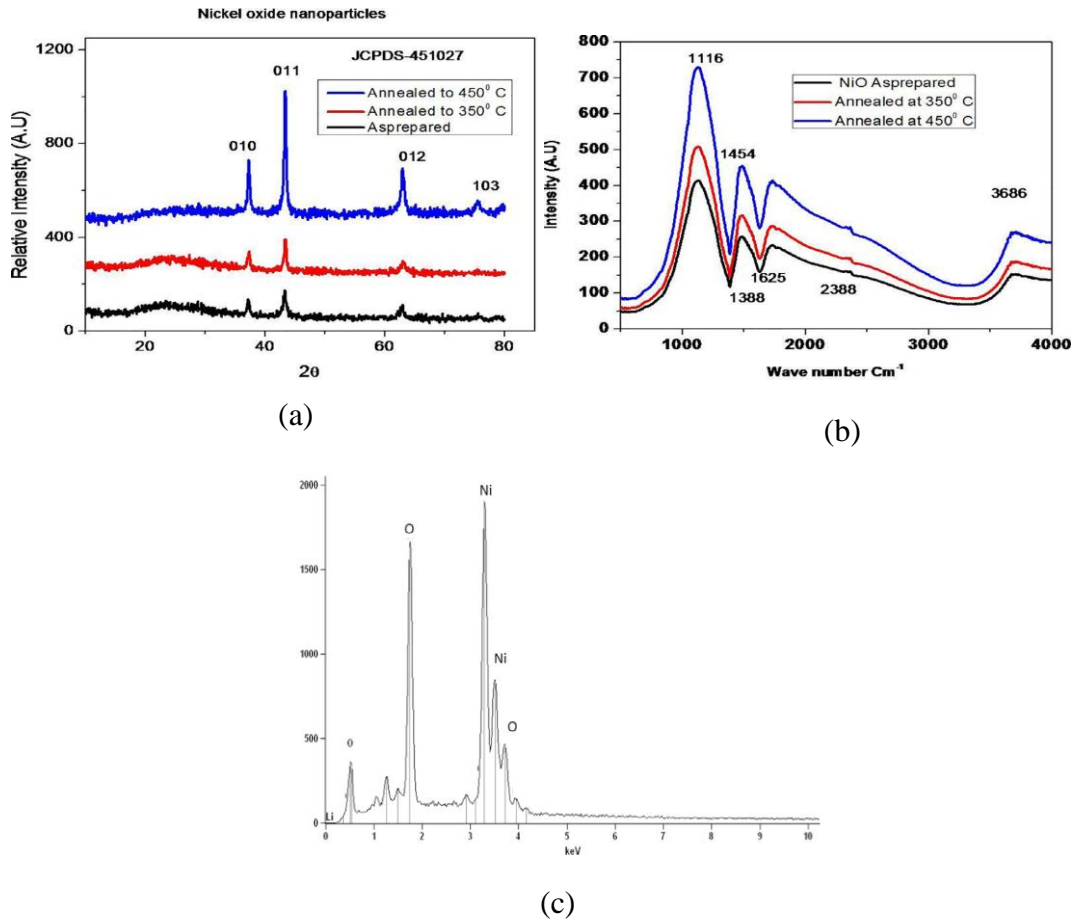


Figure 2.7 (a) XRD analysis of NiO and its two different annealing temperatures, (b) FTIR analysis of NiO (i) as-prepared (ii) 350 °C and (iii) 450 °C samples and (c) EDAX analysis of NiO NPs (Helan et al., 2016).

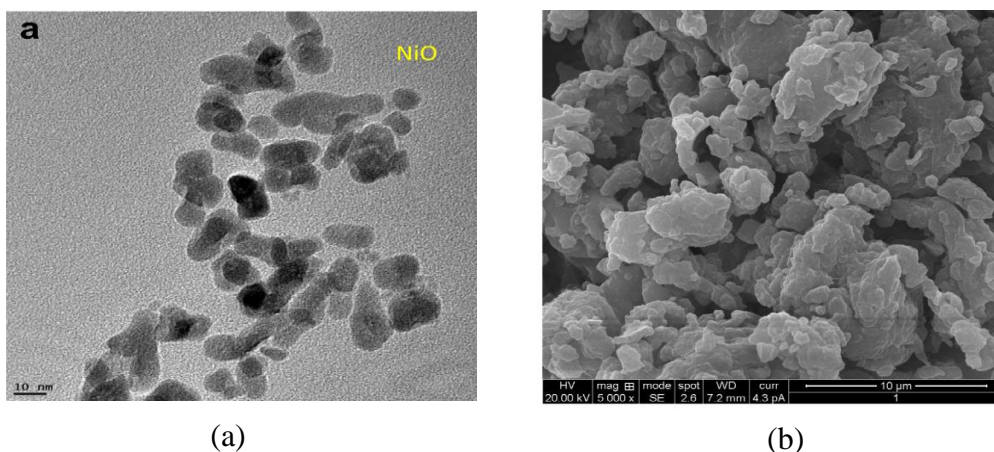


Figure 2.8 (a) TEM and (b) SEM analysis of NiO NPs (Helan et al., 2016).

Thema et al., (2016) stated that *Agathosma betulina* plant extract can be used to synthesize NiO NPs as a completely green process. The synthesized NiO NPs were characterized by HRTEM, EDS, XRD, ATR-FTIR, XPS, Raman and PL. *Agathosma betulina* plant extract can be used as an effective oxidizing/reducing agent and effective chelating chemical agent. The major chemical composition of this plant extract consists of several types of bioactive compounds such as tannins, monoterpenoids, flavonoids and triterpenoids. There are presence of nickel and oxygen in the NiO NPs as shown in the EDS spectrum in Figure 2.9 (a). The carbon coating onto the grid and its copper nature contributed to the appearance of copper and carbon elements in the EDS spectrum. From the XRD pattern shown in Figure 2.9 (b), the synthesized NiO NPs were highly crystallized single phase cubic structure with high purity. The average size of synthesized NiO NPs determined by using the Debye-Scherrer formula was 15.23 – 23.15 nm in range.

The absorption bands at 644.9 cm^{-1} and 971.0 cm^{-1} represented the Ni-O stretching vibration mode as shown in the FTIR spectrum in Figure 2.9 (c). HRTEM image (as shown in Figure 2.10) showed that the NiO NPs have average particle size to be within the range of 15 – 55 nm and slightly agglomerated particles with a certain degree of sharp edges. The average particle size of synthesized NiO NPs was found to peak at $26.7 \pm 0.4\text{ nm}$ determined by fitting the histogram data with a Gaussian distribution.

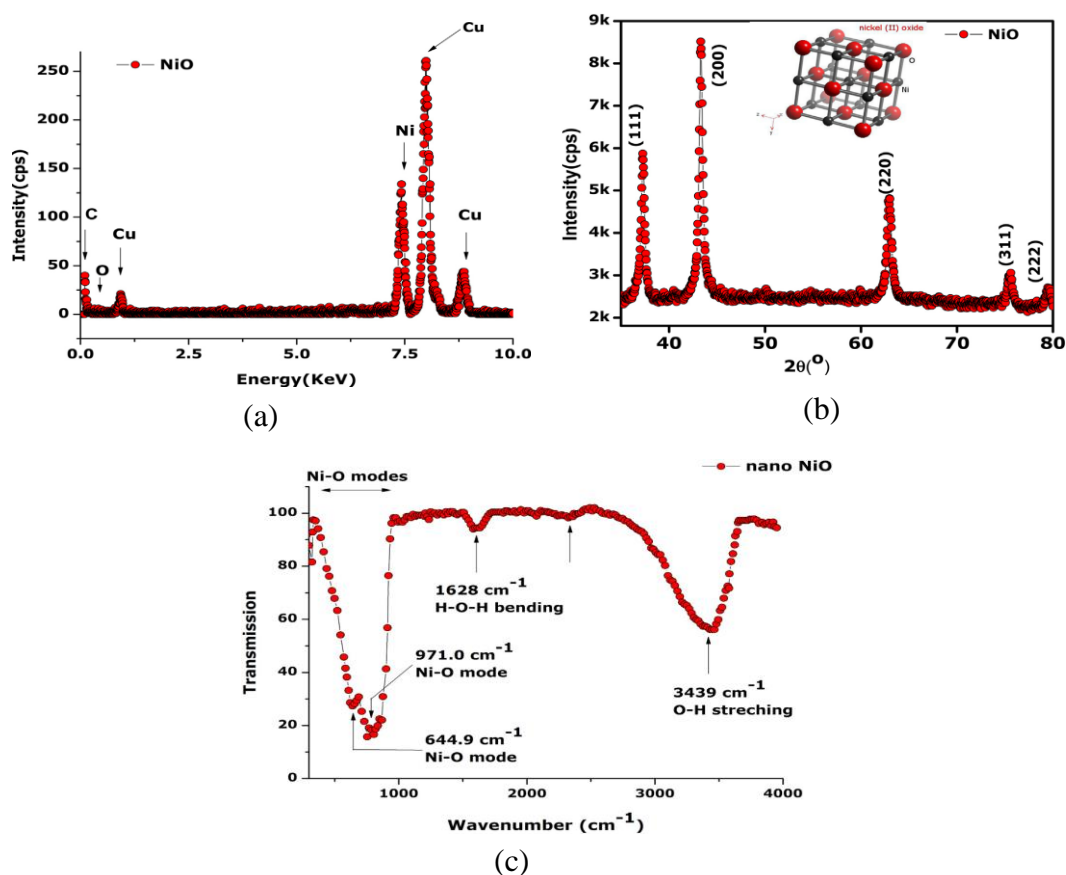


Figure 2.9 (a) EDS spectrum, (b) XRD pattern and (c) ATR-FTIR spectrum of synthesized NiO NPs (Thema et al., 2016).

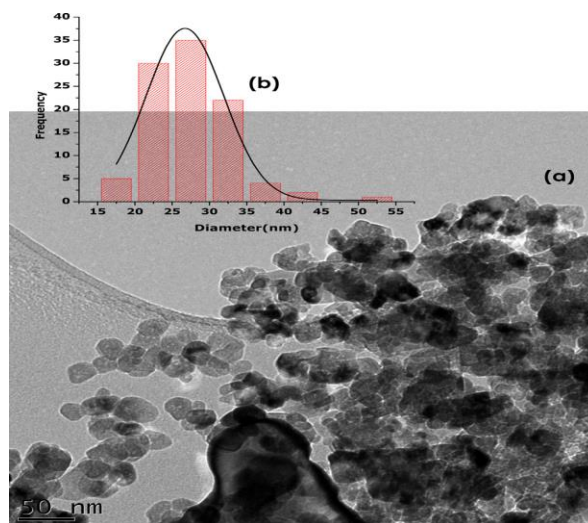


Figure 2.10 HRTEM image of synthesized NiO NPs (Thema et al., 2016).

According to Fardood, Ramazani and Moradi, (2017), NiO NPs were synthesized by using Arabic gum. The synthesized NiO NPs were characterized by FTIR, FESEM and XRD. From the FTIR spectrum shown in Figure 2.11 (a), the strong absorption band at 463.8 cm^{-1} was due to the Ni-O stretching vibration mode. The synthesized NiO NPs were in pure cubic phase with high crystallinity and average crystallite size of 34 nm as shown in the XRD pattern in Figure 2.11 (b). SEM images as shown in Figure 2.12 indicated that synthesized NiO NPs were in spherical shape with highly agglomerated.

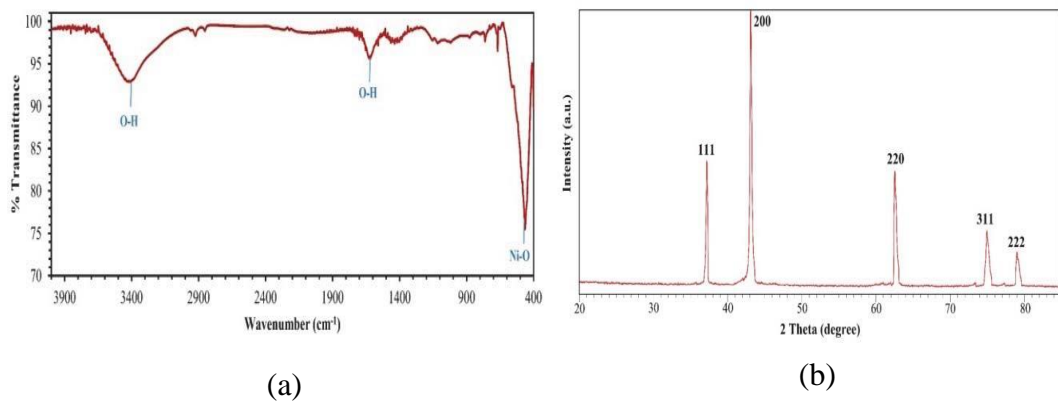


Figure 2.11 (a) FTIR spectrum and (b) XRD pattern of synthesized NiO NPs (Fardood, Ramazani and Moradi, 2017).

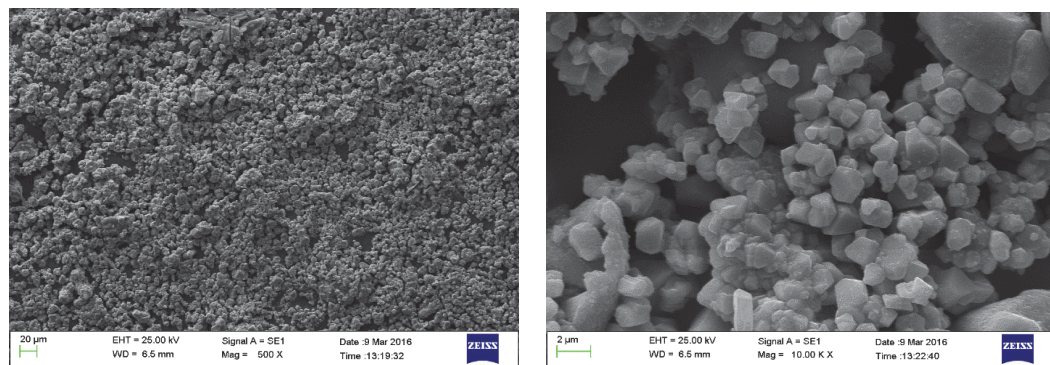


Figure 2.12 SEM images of NiO NPs (Fardood, Ramazani and Moradi, 2017).

The biosynthesis of NiO NPs by using aqueous extract of *Tamarix serotina* flowers was stated by Nasser, Ahrari and Zakerinasab, (2016). The synthesized NiO NPs were characterized by XRD, FTIR, UV-Vis, TEM, VSM and BET surface area measurements. TEM image (as shown in Figure 2.13) revealed that the NiO NPs were spherical in shapes with weak agglomeration and average particle size of 10 and 14 nm. As shown in Figure 2.14 (a), XRD pattern indicated that the NiO NPs were in cubic structure with high purity and the mean particle size calculated from Debye-Scherrer equation was 5.29 – 8.31 nm. The peak obtained at 510 cm^{-1} in the IR spectrum shown in Figure 2.14 (b) was caused by the Ni-O stretching vibration mode. A strong absorption peak was occurred at 296 nm in the UV-Visible spectrum of NiO NPs due to the n to π^* transition of Ni-O bonds. According to the BET analysis, the specific surface area of NiO NPs calculated was $126.16\text{ m}^2\text{ g}^{-1}$ while the pore size of NiO NPs calculated was 13 nm. The saturation magnetization of NiO NPs was 353 emu g^{-1} determined by the VSM analysis.

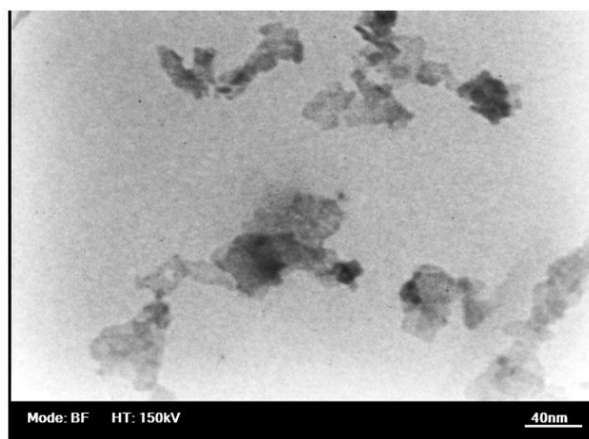


Figure 2.13 TEM image of NiO NPs (Nasser, Ahrari and Zakerinasab, 2016).

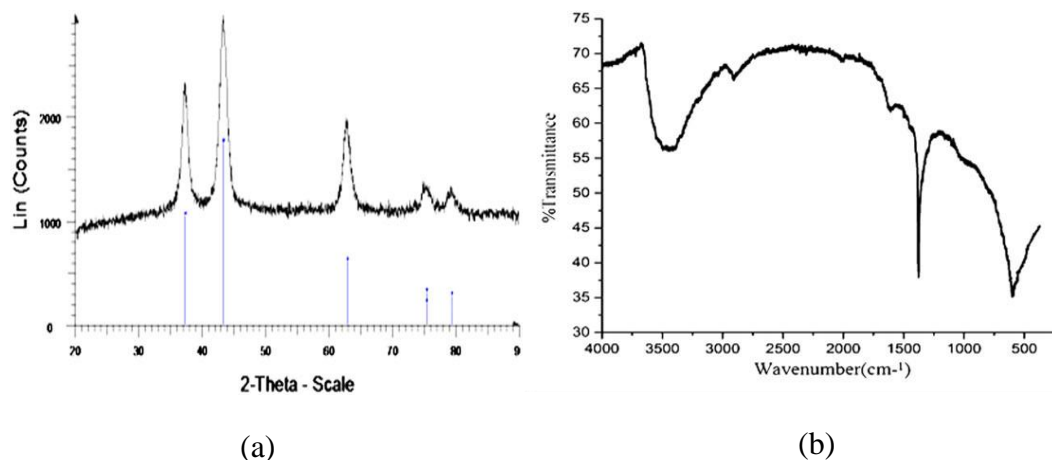


Figure 2.14 (a) XRD pattern and (b) IR spectrum of NiO NPs (Nasseri, Ahrari and Zakerinasab, 2016).

According to Mariam et al., (2014), NiO NPs were synthesized by using leaves of *Psidium guajava*. The synthesized NiO NPs were characterized by XRD, FESEM, TEM, UV-Vis and magnetic measurements. From the TEM image shown in Figure 2.15 (a), the synthesized NiO NPs were in spherical shapes with particle size of less than 100 nm. The NiO NPs were found to be in spherical shape and highly agglomerated with the particle size range of 17 – 70 nm in SEM image as shown in Figure 2.15 (b). XRD pattern as shown in Figure 2.16 confirmed the synthesized NiO NPs were pure cubic face centered with an average crystallite size of 22 and 44 nm. From the absorbance spectra as shown in Figure 2.17 (a), the band gap values of NiO NPs was at 327 nm as proved by the absorbance value of 0.2 – 0.8 Å. The direct band gap value of NiO NPs determined from the Tauc plot shown in Figure 2.17 (b) was 2.69 eV. The magnetic flux density value of

NiO NPs determined was found to be 60 emu/g. The synthesized NiO NPs showed *in vitro* cytotoxic effect against HT-29 cell lines.

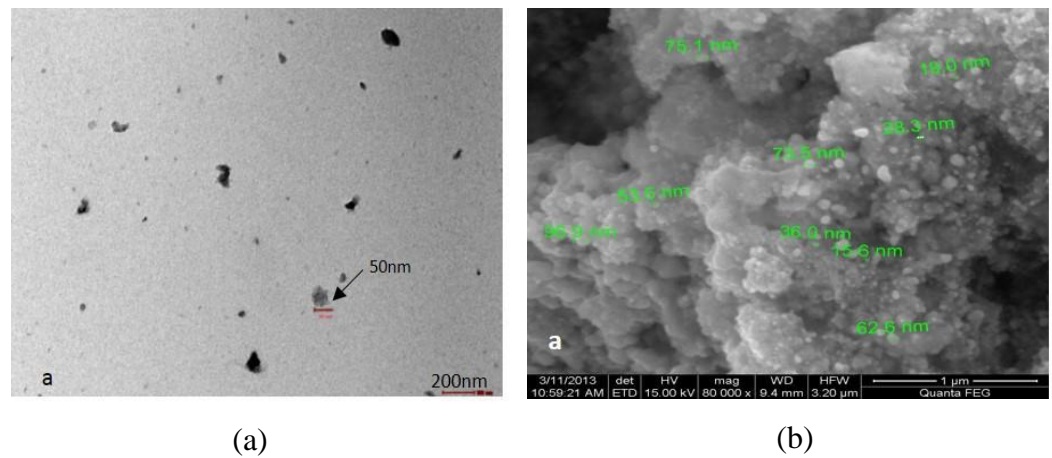


Figure 2.15 (a) TEM image and (b) SEM image of biosynthesized NiO NPs (Mariam et al., 2014).

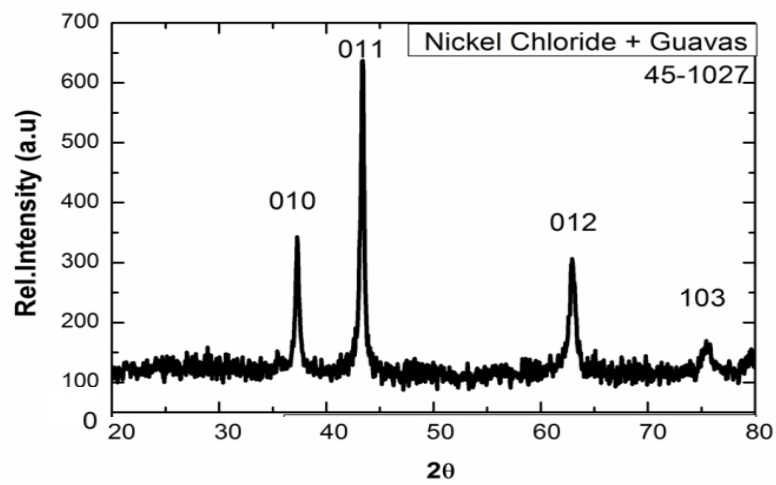
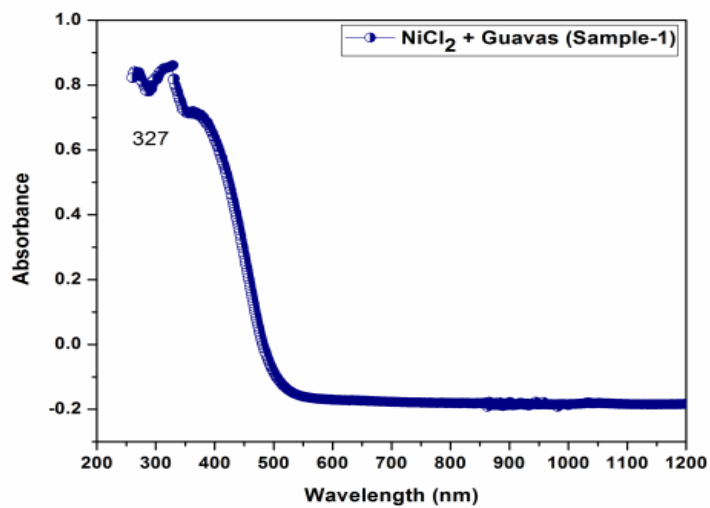
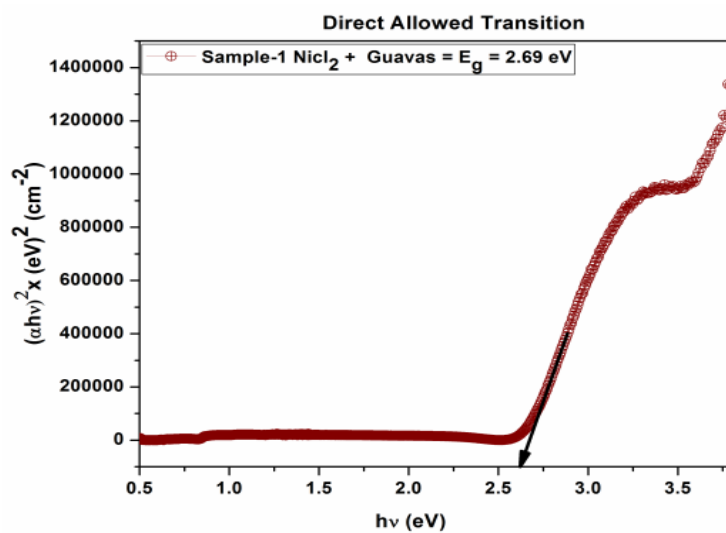


Figure 2.16 XRD pattern of biosynthesized NiO NPs (Mariam et al., 2014).



(a)



(b)

Figure 2.17 (a) Absorbance spectra and (b) Tauc plot of biosynthesized NiO NPs

(Mariam et al., 2014).

Azhagu Raj, AlSalhi and Devanesan, (2017) reported that the use of *Coriandrum sativum* leaf extract to synthesize NiO NPs, assisted by microwave method. The synthesized NiO NPs were characterized by XRD, SEM, TEM, XPS, BET analysis and VSM. XRD pattern (as shown in Figure 2.18) confirmed the high crystallinity single phase structure of pure cubic NiO NPs with average crystallite size of 15.66 nm by using Debye-Scherrer's method. As shown in Figure 2.19 (a,b), HRSEM images revealed that the NiO NPs were in spherical shape with highly agglomerated particles. From HRTEM images shown in Figure 2.20 (a,b), NiO NPs were found to be highly crystalline and almost spherical in shape with a homogeneous distribution. The surface area, pore volume and average pore diameter for NiO NPs produced via microwave method were determined to be $60.35 \text{ m}^2 / \text{g}$, $0.9427 \text{ cm}^3 / \text{g}$ and 13.27 \AA respectively. The authors also reported that the synthesized NiO NPs possessed antibacterial properties against human Gram-positive and Gram-negative bacterial pathogens.

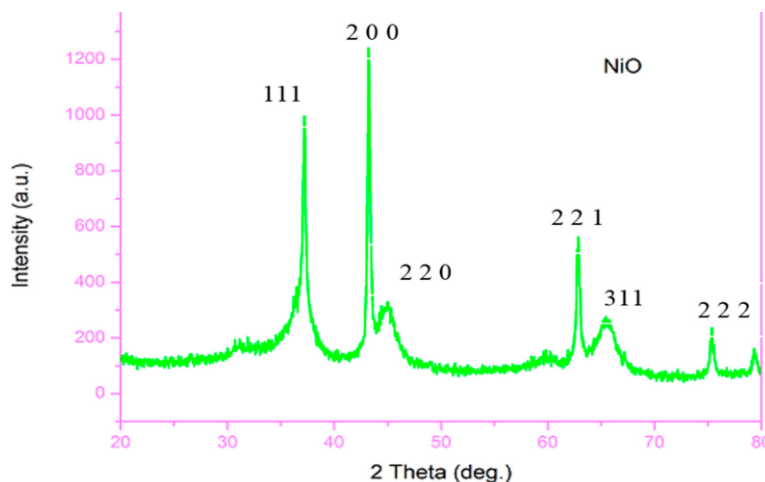


Figure 2.18 XRD pattern of NiO NPs (Azhagu Raj, AlSalhi and Devanesan, 2017).

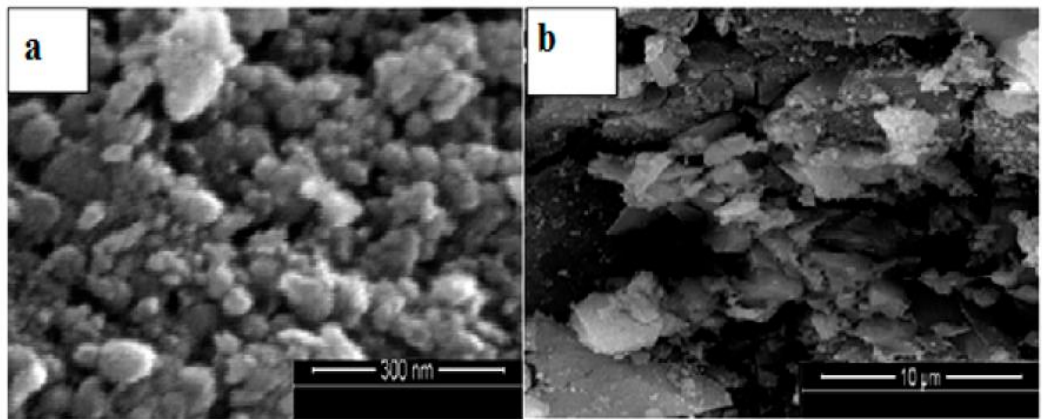


Figure 2.19 (a,b) HRSEM images of NiO NPs (Azhagu Raj, AlSalhi and Devanesan, 2017).

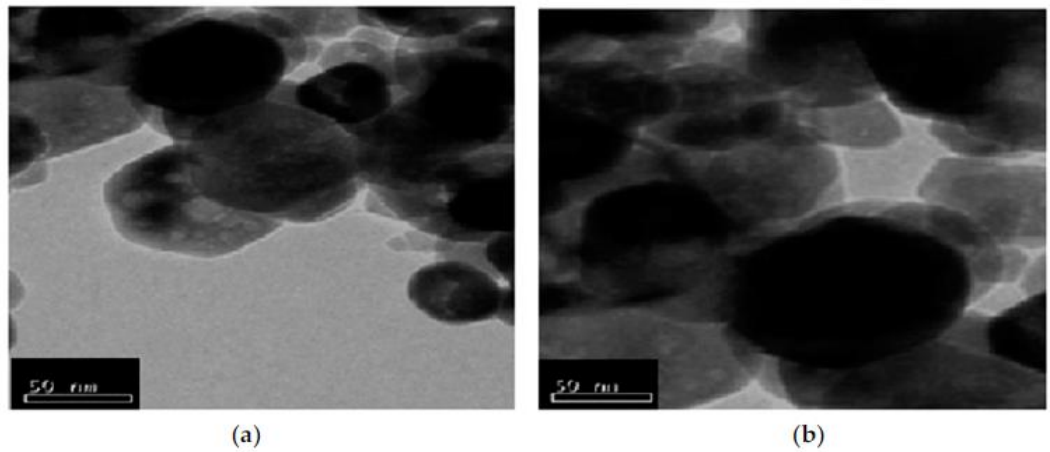


Figure 2.20 (a,b) HRTEM images of NiO NPs (Azhagu Raj, AlSalhi and Devanesan, 2017).

2.1.2 Synthesis of NiO NPs by using Microorganisms

The biosynthesis of NiO NPs extracellularly by using fungus *Fusarium verticillioides* (Sacc.) was reported by El-Debaiky, El-Badry and El-Shahawy, (2017). The synthesized NiO NPs were characterized by XRD, TEM and FTIR. According to XRD pattern shown in Figure 2.21, it showed that single phase NiO NPs possessed a face centered cubic of polycrystalline structure with average crystallite size of 8 – 17.7 nm when annealed at 400 °C and 600 °C, respectively. TEM images (as shown in Figure 2.22) revealed that the NiO NPs were in spherical shape with average particle size found to be about 8.5 nm when annealed at 400 °C and 20.7 nm when annealed at 600 °C. From the FTIR spectra shown in Figure 2.23, the absorption band at 439 cm⁻¹ and 555 cm⁻¹ were assigned to Ni-O and Ni-O-H stretching mode. The biosynthesized NiO NPs have significant effect on antifungal activity against the causative species of mycotic keratitis, with good washing out rates which do not accumulate within animal tissues and have high penetration rates. The minimum inhibitory concentration (MIC) of NiO NPs was reported in the range of 12.5 – 25 mg/mL.

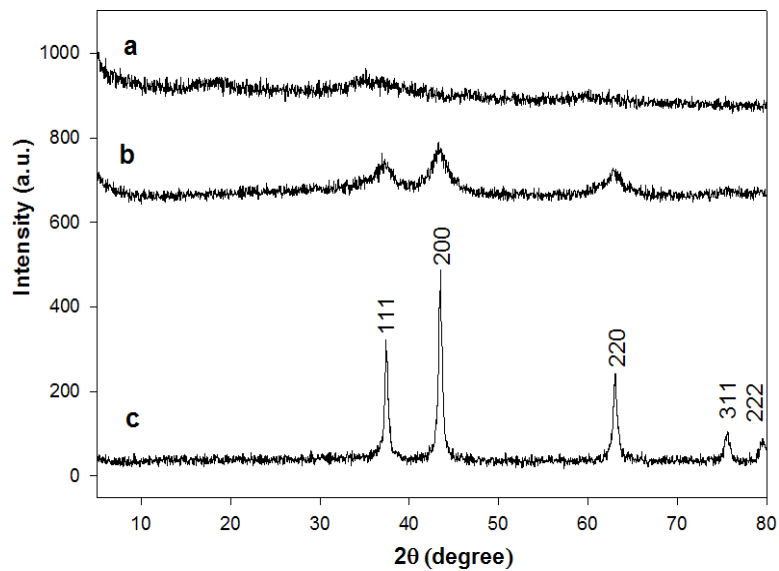


Figure 2.21 XRD pattern of NiO NPs (a) as prepared, (b) after annealing at 400 °C and (c) after annealing at 600 °C (El-Debaiky, El-Badry and El-Shahawy, 2017).

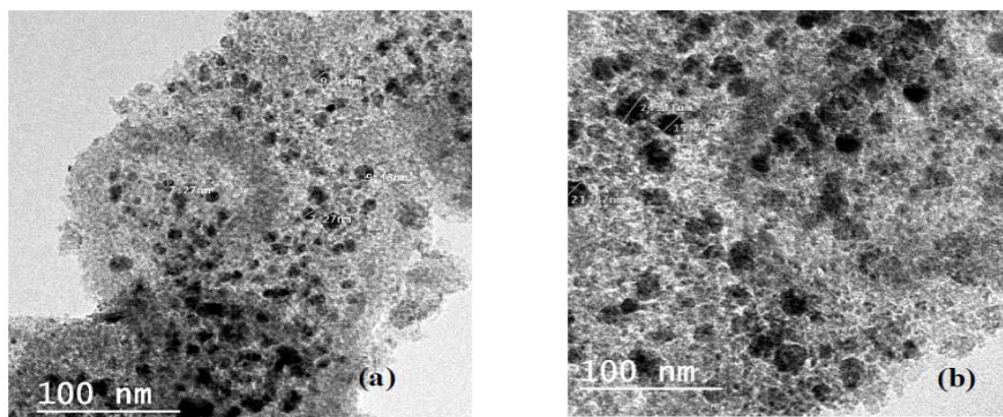


Figure 2.22 TEM images of annealed NiO NPs (a) at 400 °C and (b) at 600 °C (El-Debaiky, El-Badry and El-Shahawy, 2017).

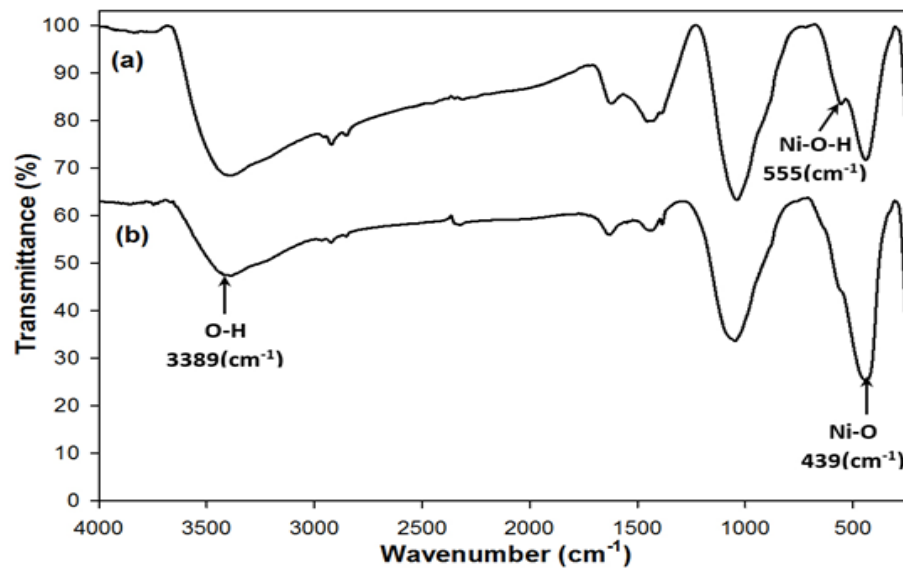


Figure 2.23 FTIR spectra of annealed NiO NPs (a) at 400 °C and (b) at 600 °C (El-Debaiky, El-Badry and El-Shahawy, 2017).

CHAPTER 3

METHODOLOGY

3.1 Chemicals

Carica Papaya was purchased from night market Kampar, Perak, Malaysia. Nickel(II) nitrate hexahydrate $[\text{Ni}(\text{NO}_3)_2 \cdot 6\text{H}_2\text{O}]$ salt precursor which is the starting material for synthesis of NiO NPs was purchased from Alfa Aesar Chemical Manufacturing Company and used without any further purification. Methylene blue is a dye that was purchased from R&M Chemicals and used without further purification. All glassware were rinsed with distilled water and dried in a hot air oven before use.

3.2 Green Synthesis of Nickel Oxide Nanoparticles

3.2.1 Preparation of *Carica Papaya* Peel Extract

Carica Papaya peel was first thoroughly washed with tap water and then rinsed several times with deionized water to properly remove all the dust and unwanted visible particles. About 150 g of peel was weighed and then finely cut into small pieces by using a knife. 150 mL of deionized water was heated to 70 – 80 °C in a 500 mL beaker and then the peel was added into it. The solution was heated for 30 minutes and the temperature was maintained at 70 – 80 °C. After that, the solution was cooled down and filtered twice through Whatman No.1 filter paper on filter funnel to obtain a clear yellowish-orange solution of papaya peel extract. The extract was directly used in the next step of the synthesis part.

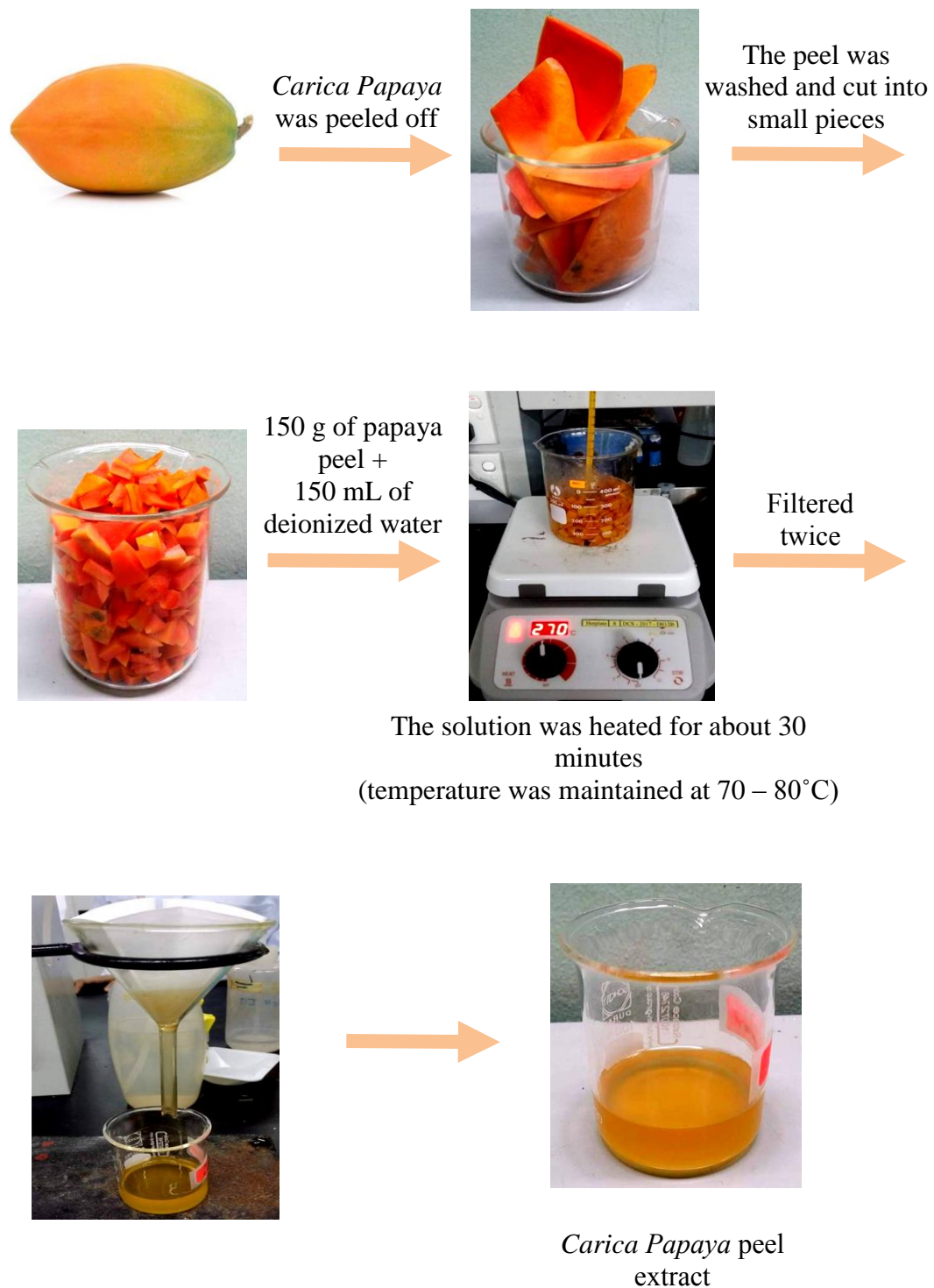


Figure 3.1 Preparation of *Carica Papaya* Peel Extract.

3.2.2 Synthesis Process of NiO NPs

50 mL of *Carica Papaya* peel extract was heated to 70 – 80 °C in a 100 mL beaker. After that, about 1 g of nickel(II) nitrate hexahydrate [Ni(NO₃)₂·6H₂O] was added into it. The solution was maintained at a constant temperature of 70 – 80 °C under continuous stirring on magnetic stirring hotplate. A colour change of the solution from yellowish-orange to light green and lastly turned into dark green indicated the formation of nickel atoms. The solution was heated until it formed a dark green colored paste. The paste was then transferred into a ceramic crucible and then calcinated in the Nabertherm furnace at 450 °C for 2 hours in air to get NiO NPs. The NiO NPs produced were ground into finely divided particles by using mortar and pestle. Finally, a greyish-black colored powder was obtained. The NiO NPs were then placed in the sample vial for the purpose of dye degradation process and further characterization analysis.

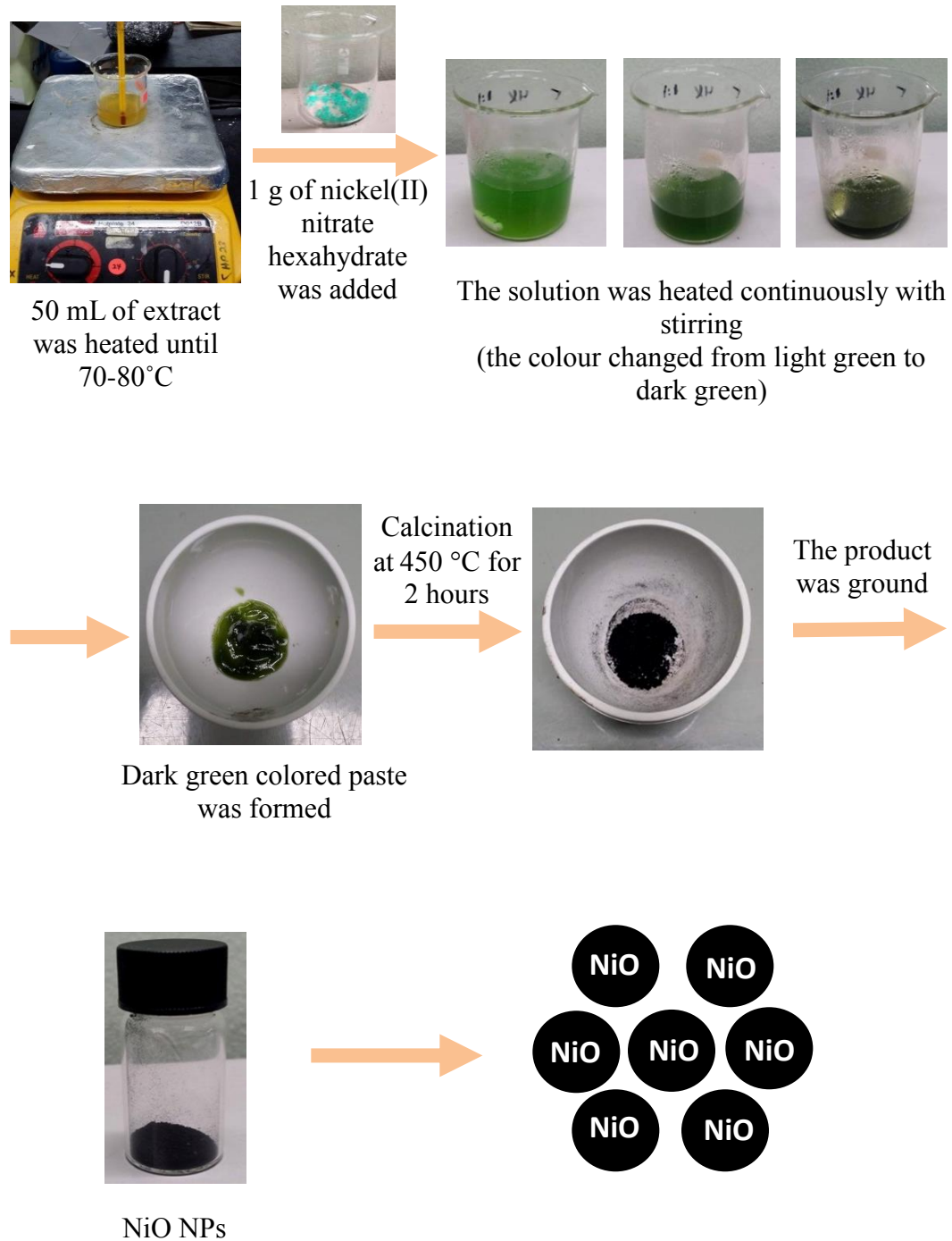


Figure 3.2 Synthesis of NiO NPs using *Carica Papaya* Peel Extract.

3.3 Characterization of Synthesized Nickel Oxide Nanoparticles

The synthesized NiO NPs were characterized using Ultraviolet-Visible Spectroscopy (UV-Vis), Fourier Transform Infrared Spectroscopy (FTIR), Energy Dispersive X-ray Spectroscopy (EDX), X-ray Diffraction (XRD) and Scanning Electron Microscopy (SEM).

X-ray Diffraction (XRD) was used to identify the crystalline characteristics, crystalline structure and its crystalline size and phases of the synthesized NiO NPs by using Shimadzu XRD 6000 Diffractometer with Cu K α radiation (Voltage = 40 kV, Current = 30 mA, $\lambda = 1.5406 \text{ \AA}$, scan rate of 2.0 min^{-1} and scan range of 2θ from 10° – 80°). The XRD was performed by the penetration of X-rays into the synthesized NiO NPs and the resulting diffraction pattern is compared with standards to obtain structural information of synthesized NiO NPs. From the XRD data obtained, the average crystallite size of synthesized NiO NPs was calculated by using the Debye-Scherrer Equation (3.1) as shown below:-

$$D = \frac{k \lambda}{\beta \cos \theta} \quad (3.1)$$

where,

D = Average crystalline diameter size

k = Scherrer constant (usually 0.9)

λ = Wavelength of X-ray source, (Cu K α radiation = 1.5406 \AA)

β = Full width at half-maximum (FWHM) of the X-ray diffraction peak in radian
 2θ

θ = Bragg's diffraction angle

β obtained from the XRD data was converted to radian unit by using the equation (3.2) as shown below:-

$$\beta = \frac{\text{FWHM in } 2\theta \times \pi}{180^\circ} \quad (3.2)$$



Figure 3.3 Shimadzu XRD 6000.

Fourier Transform Infrared Spectroscopy (FTIR) was used for characterizing the organic functional groups (e.g. carbonyls, hydroxyls) attached to the surface of *Carica Papaya* peel extract and synthesized NiO NPs. FTIR spectra of papaya peel extract and the synthesized NiO NPs were recorded and compared using Perkin Elmer Spectrum RX1 Fourier Transform Infrared Spectrometer using KBr pellet technique scanning from 4000 cm^{-1} to 400 cm^{-1} . The papaya peel extract was pre-frozen in the $-18\text{ }^{\circ}\text{C}$ freezer overnight before carried out the freeze-drying process for 8 nights until it was completely dried in a powder form before subjected to FTIR analysis.



Figure 3.4 Perkin Elmer Spectrum RX1 Fourier Transform Infrared Spectrometer.

Ultraviolet-Visible Spectroscopy (UV-Vis) was used to evaluate the optical properties of synthesized NiO NPs by using UV-Vis Single Beam Spectrophotometer (Thermo Fischer Scientific Genesys 10S series UV-Visible spectrophotometer) which scanning in the range of 200 to 800 nm. It is an important method to detect the formation and stability of NiO NPs in the reaction mixture of papaya peel extract with nickel(II) nitrate hexahydrate. The deionized water was used as a blank in all the measurements. In the dispersion process, sample solution was prepared by dispersing 10 mg of synthesized NiO NPs in 10 mL of deionized water in sonicator for about 30 minutes. Sonication is a process of converting an electrical signal into a physical vibration in order to agitate particles in solution.

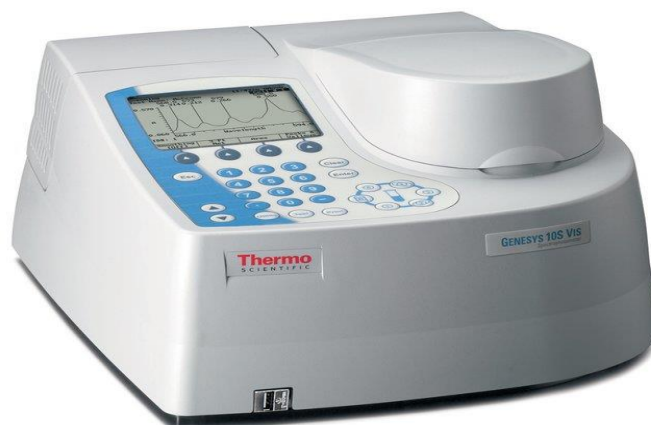


Figure 3.5 UV-Vis Single Beam Spectrophotometer (Thermo Fischer Scientific Genesys 10S Series UV- Visible Spectrophotometer).

Scanning electron microscopy (SEM) was used to determine the surface morphology and topography of synthesized NiO NPs and investigate the shape, size and the surface area of synthesized NiO NPs at the nanometer scale by using Scanning Electron Microscope (JEOL JSM-6701F).



Figure 3.6 Scanning Electron Microscope (JEOL JSM-6701F).

Energy Dispersive X-ray Spectroscopy (EDX) was used to determine the elemental composition of synthesized NiO NPs by using Oxford Instrument X-Max Energy Dispersive X-ray Diffractometer.



Figure 3.7 Energy Dispersive X-Ray Diffractometer.

3.4 Photocatalytic Activity of Synthesized Nickel Oxide Nanoparticles

3.4.1 Preparation of Methylene Blue (MB) Dye Aqueous Solutions

10 ppm of MB dye solution was prepared by dissolving about 10 mg of MB powder using deionized water in a beaker. The solution was then poured into a 1 L volumetric flask and then topped up to the line with deionized water. The volumetric flask was wrapped with the aluminum foil to prevent the photo-degradation of MB molecules.

3.4.2 Photocatalytic Dye Degradation of Methylene Blue (MB) using synthesized NiO NPs as a function of time

About 50 mg of synthesized NiO NPs was added into 100 mL beaker which containing 50 mL of MB dye aqueous solution. A total of nine beakers were prepared using the same amount of synthesized NiO NPs and same volume of MB dye aqueous solution. Then, each beaker was magnetically stirred in the dark for about 30 minutes on magnetic stirring hotplate. This to ensure that the synthesized NiO NPs and MB dye aqueous solution are homogeneous and reach adsorption/desorption equilibrium of MB dye on the catalyst surface of NiO NPs. After that, the beakers were placed under the sunlight to expose to the UV irradiation and the samples were collected based on the different time intervals as shown in Table 3.1. The most suitable time for the exposure to sunlight is at 11

am to 4 pm because the light intensity is the strongest within this range of time. However, the sunlight intensity was measured by using lightmeter (Sper Scientific UVA/B Light Meter 850009) at every 1 hour interval in order to maintain the light intensity in the range of 9 – 13 mW/cm². At certain time intervals, the dye sample solutions were collected into a centrifuge tube. The dye sample solutions were then centrifuged by using Centrifuge 5430 at a speed of 7830 rpm for 5 minutes in order to separate the dye solution from photocatalyst. After centrifugation process, the supernatant were collected using dropper and transferred into cuvette in order to measure the absorbance in the range of the wavelength from 200 nm to 800 nm by using UV-Vis Single Beam Spectrophotometer in order to monitor the photocatalytic degradation process of MB. The maximum wavelength, λ_{max} of MB was recorded as 665 nm.

Table 3.1 Time intervals during dye degradation process.

Number of Beakers	Time (minutes)
	MB Dye Aqueous Solution
1	Control
2	30
3	60
4	90
5	120
6	150
7	180
8	210
9	320

3.4.3 Determination of Percentage of Degradation

$$\text{Percentage of Dye Degradation} = \frac{A_0 - A_t}{A_0} \times 100\% \quad (3.3)$$

where,

A_0 = Initial absorbance of dye solution before expose to sunlight

A_t = Absorbance of dye solution after photocatalytic degradation at different irradiation time (t)

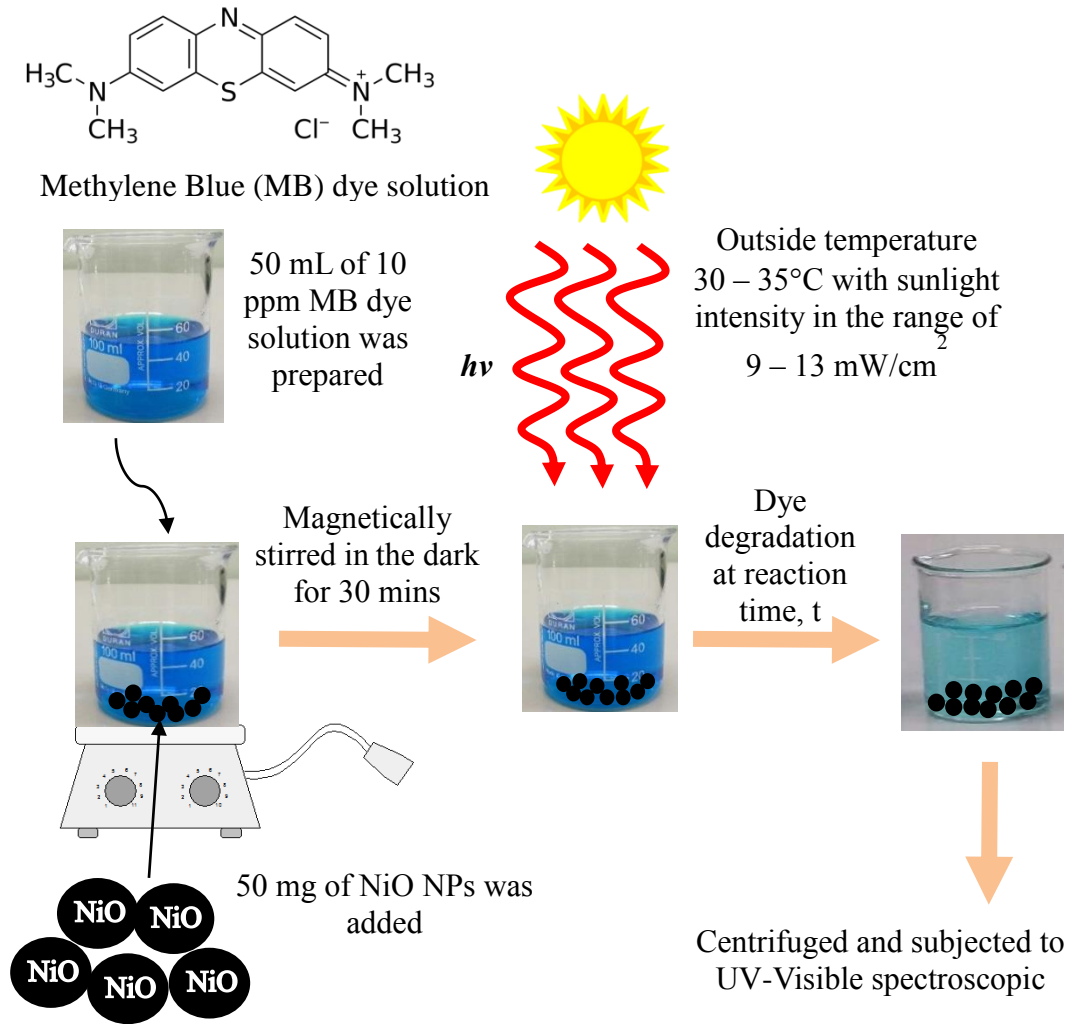


Figure 3.8 Photocatalytic activity of synthesized NiO NPs under solar irradiation.

CHAPTER 4

RESULTS AND DISCUSSION

4.1 Green Synthesis of Nickel Oxide Nanoparticles

Greyish-black NiO NPs were successfully synthesized by using *Carica Papaya* peel extract as shown in Figure 4.1. Green synthesis of NiO NPs using papaya peel extract helps to reduce significant amount of waste produced to the environment. This fulfilled the Principle 1 in the 12 Principles of Green Chemistry, which is to prevent waste. The use of papaya peel extract as starting materials in the synthesis of NiO NPs is considered green as it is the agricultural waste and thus it fulfilled the Principle 4 in the 12 Principles of Green Chemistry, which is the safer chemicals and products. Deionized water (universal green solvent) was used as the solvent instead of volatile organic solvent (VOC) throughout the whole NiO NPs synthesis process. This process can be considered as a green synthetic route as it fulfilled the Principle 5 in the 12 Principles of Green Chemistry, which is the safer solvents and reaction conditions. Since the reaction was carried out in a mild condition which means conducted at room temperature, therefore it is low energy consumption and it fulfilled the Principle 6 in the 12 Principles of Green Chemistry, which is increase energy efficiency. The synthesized NiO NPs produced in the process are non-toxic and non-hazardous to

the people and the environment so it fulfilled the Principle 3 in the 12 Principles of Green Chemistry, which is less hazardous chemical syntheses.



Figure 4.1 Photograph of NiO NPs synthesized using *Carica Papaya* peel extract.

The synthesis of NiO NPs involved a redox process. NiO NPs was synthesized by the reaction of nickel(II) nitrate hexahydrate with *Carica Papaya* peel extract. The peel extract acts as a reducing agent and stabilizing agent in this synthesis process. The biomolecules components such as flavonoids, alkaloids, proteins, tannins, terpenoids, phenolic compounds present in the peel extract are responsible for the reduction of nickel ions to nickel nanoparticles. The peel extract also act as a capping agent in order to maintain the size of particles formed in nano scale. Reduction of the nickel ion, Ni(II) to nickel atom, Ni(0) (Ni^{2+} to Ni^0) happened during the reaction. This reduction process occurred was confirmed by the change in colour of the solution from yellow to light green then become dark green and finally a dark green coloured paste was formed indicated the formation of colloidal nickel nanoparticles. After a period of times, there was no further change in the colour of the solution indicating that the whole nickel salt present in the solution have been reduced. A color change from dark green

coloured paste to greyish-black coloured powder upon thermal decomposition was observed indicating the formation of NiO NPs. The chemical reactions are shown in the equation below:-



4.2 Characterization of Synthesized Nickel Oxide Nanoparticles

The synthesized NiO NPs were characterized using Ultraviolet-Visible Spectroscopy (UV-Vis), Fourier Transform Infrared Spectroscopy (FTIR), Energy Dispersive X-ray Spectroscopy (EDX), X-ray Diffraction (XRD) and Scanning Electron Microscopy (SEM).

4.2.1 X-ray Diffraction (XRD)

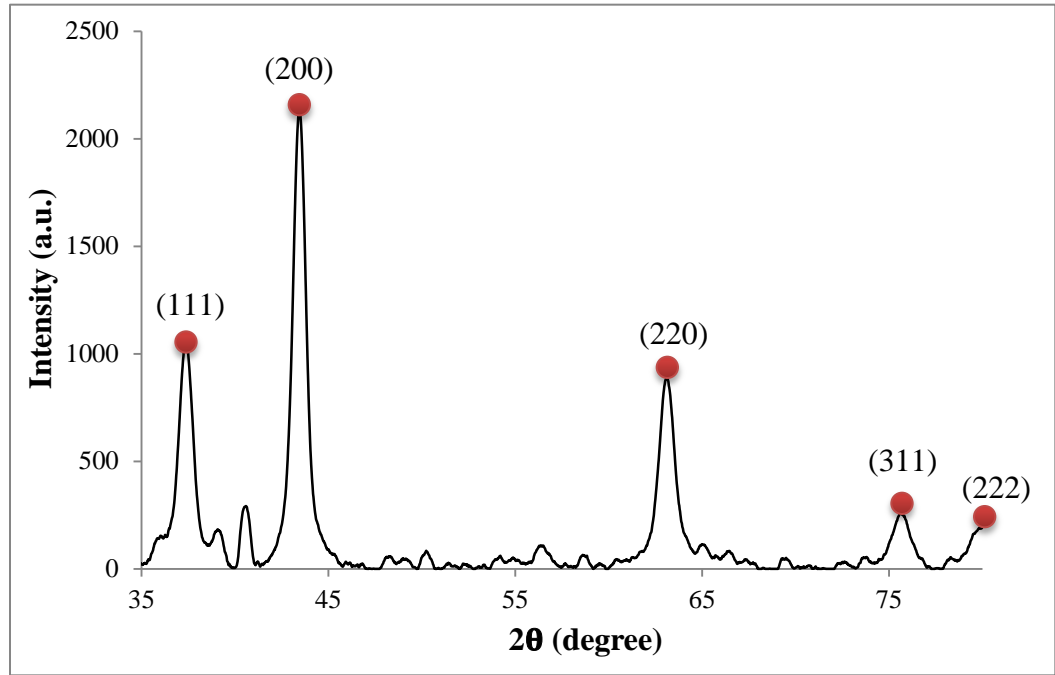


Figure 4.2 XRD pattern of synthesized NiO NPs.

The five distinct separate diffraction peaks in the XRD pattern shown in Figure 4.2 at $2\theta = 37.38^\circ$, 43.45° , 63.11° , 75.65° and 79.84° can be indexed to (111), (200), (220), (311) and (222) crystal planes, respectively. All the diffraction peaks obtained were in accordance with the Joint Committee Powder Diffraction Standards (JCPDS card No. 73-1523). This indicated that the synthesized NiO NPs were single crystalline which having face centered cubic phase. Similar results were also reported by Ezhilarasi et al., (2016), where the diffraction peaks at $2\theta = 37.25^\circ$, 43.26° , 63.11° , 75.46° and 79.45° corresponded to the (111), (200), (220), (311) and (222) crystal planes, respectively. The broadening of the diffraction peaks indicated the formation of NiO nanocrystalline phase (Helan et

al., 2016). There are some of the minor and unassigned peaks occurred in the XRD pattern might be due to the presence of impurities in the synthesized NiO NPs or may be related to the crystallization of bioorganic phases present in papaya peel extract on the surface of the synthesized NiO NPs. The average crystallite size of synthesized NiO NPs determined from the FWHM of highest intense peak corresponding to (200) plane at 43.45° was found to be 13.39 nm from the XRD pattern according to Debye-Scherrer equation as shown in Appendix A. The ability of papaya peel extract to be act as a fuel and capping agent able to reduce the size of the particle of NiO and thus the crystallite size of NiO NPs can be reduced.

4.2.2 Energy Dispersive X-ray Spectroscopy (EDX)

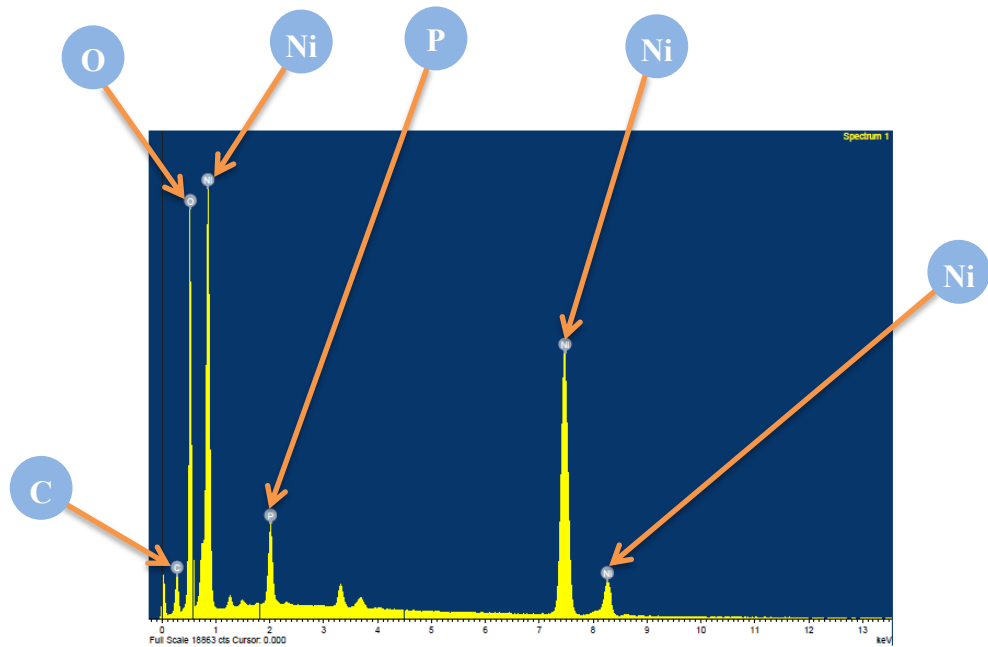


Figure 4.3 EDX spectrum of synthesized NiO NPs.

Table 4.1 EDX analysis processing data.

Elements	Weight %	Atomic %
C	13.02	24.86
O	38.32	54.93
P	3.42	2.54
Ni	45.24	17.67
Total	100.00	100.00

From the EDX spectrum shown in Figure 4.3, there are a total of four elements present in the synthesized NiO NPs which are carbon, oxygen, phosphorus and nickel. The spectrum showed the presence of elemental Ni as the major constituent with weight % of 45.24. It also indicated that the synthesized NiO NPs were mainly composed of Ni and O elements as Ni and O peaks are majorly visible in the spectrum. This confirmed the formation of nano-scaled oxide is NiO NPs. The carbon present with the weight % of 13.02 was due to the biomolecules components in the papaya peel extract that served as capping agent which surrounded on the NiO NPs surface. Trace amount of phosphorus was also found with weight % of 3.42 because the papaya peel which used to synthesize NiO NPs was rich in phosphorus.

4.2.3 Fourier Transform Infrared Spectroscopy (FTIR)

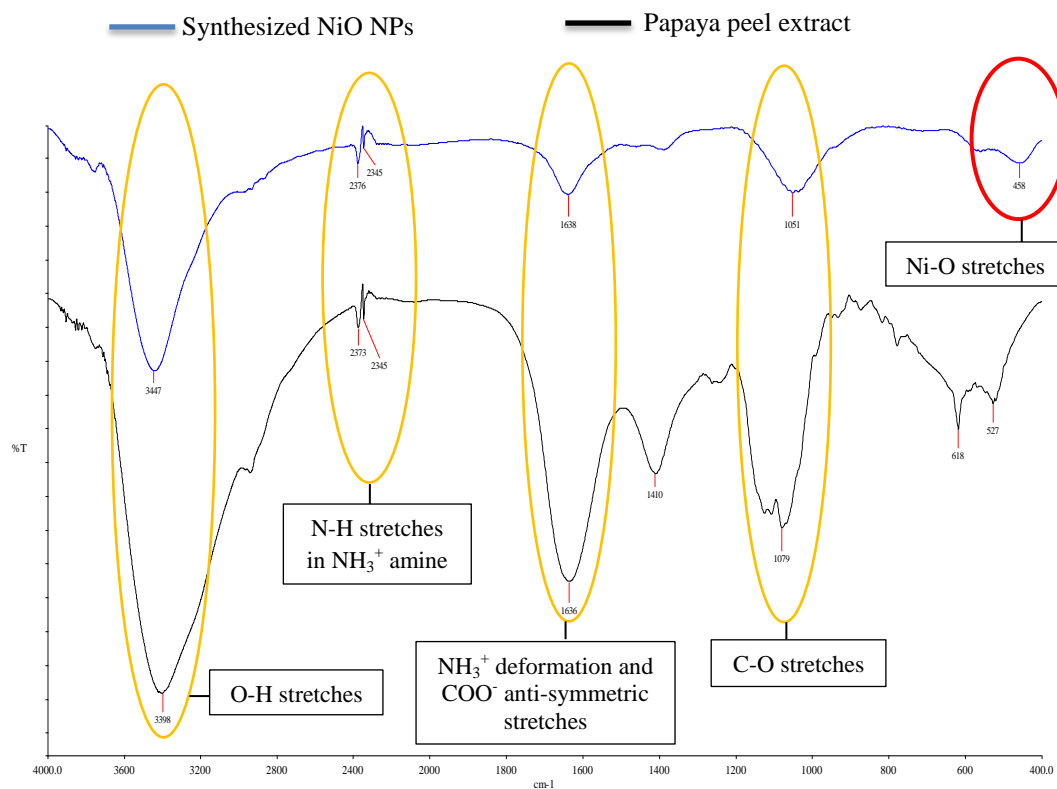


Figure 4.4 FTIR comparative spectra of synthesized NiO NPs and papaya peel extract.

FTIR spectra comparison between synthesized NiO NPs and papaya peel extract were shown in Figure 4.4. The absorption bands below 1000 cm⁻¹ generally belong to metal oxides arising from interatomic vibrations (Sharma et al., 2015). In the IR spectrum of synthesized NiO NPs, the peak at 458 cm⁻¹ corresponded to the Ni-O stretching vibration mode which further confirmed the formation of NiO NPs. The broadness of this peak indicated that the NiO NPs are nanocrystals (El-

Debaiky, El-Badry and El-Shahawy, 2017). The broad and strong absorption bands at 3447 cm^{-1} and 1638 cm^{-1} in IR spectrum of synthesized NiO NPs attributed to the adsorptions of water molecules onto the NiO NPs surface when samples are exposed to the atmosphere while the broad absorption bands at 3398 cm^{-1} and 1636 cm^{-1} in IR spectrum of papaya peel extract corresponded to the deformation vibration of the adsorbed water molecules (Fardood, Ramazani and Moradi, 2017). The broad absorption bands appeared at 3447 cm^{-1} and 3398 cm^{-1} in IR spectrum of synthesized NiO NPs and papaya peel extract respectively were mainly the O-H stretching vibration mode. The presence of hydroxyl group shown in IR spectrum of papaya peel extract was due to phenolic compounds present in the papaya peel extract.

The sharp absorption bands at 2376 cm^{-1} and 2345 cm^{-1} for IR spectrum of synthesized NiO NPs and 2373 cm^{-1} and 2345 cm^{-1} for IR spectrum of papaya peel extract were due to the N-H stretching vibrational mode in $-\text{NH}_3^+$ amine. There are also antisymmetric stretching and symmetric stretching mode of vibrations of CO_2 molecule occurred at the peak of 2376 cm^{-1} and 2345 cm^{-1} in IR spectrum of synthesized NiO NPs due to CO_2 inside the grains of the nanoparticles or aerial CO_2 (Ezhilarasi et al., 2016). The presence of H_2O and CO_2 stretching vibration mode showed that the rapid adsorption of water and carbon dioxide of NiO NPs from the atmosphere which in turns indicated that the NiO NPs possessed high surface area.

The peak at 1638 cm^{-1} and 1636 cm^{-1} in IR spectrum of synthesized NiO NPs and papaya peel extract respectively represented the bending mode of hydroxyl group and water molecules. These observations showed the effect of hydration in the structure. Those absorption peak also associated with stretching vibration of C=C bond of aromatic rings and assigned to NH_3^+ deformation of NH_3^+ in amino acids or anti-symmetric stretching vibrations of carboxylic acid salt (COO^-). The absorption peak at 1051 cm^{-1} and 1079 cm^{-1} in IR spectrum of synthesized NiO NPs and papaya peel extract respectively belonged to C-O stretching vibrational mode. Other minor peaks appeared in IR spectrum of papaya peel extract indicated that the extract contains of proteins, terpenoids and other secondary metabolites (Donda et al., 2013).

Shifting of these following peaks were observed in IR spectrum of NiO NPs such as 3398 cm^{-1} to 3447 cm^{-1} , 2373 cm^{-1} to 2376 cm^{-1} , 1636 cm^{-1} to 1638 cm^{-1} and 1079 cm^{-1} to 1051 cm^{-1} indicated that carboxyl, carbonyl, hydroxyl and amide group in papaya peel extract was taking part in the synthesis of NiO NPs.

4.2.4 Ultraviolet-Visible Spectroscopy (UV-Vis)

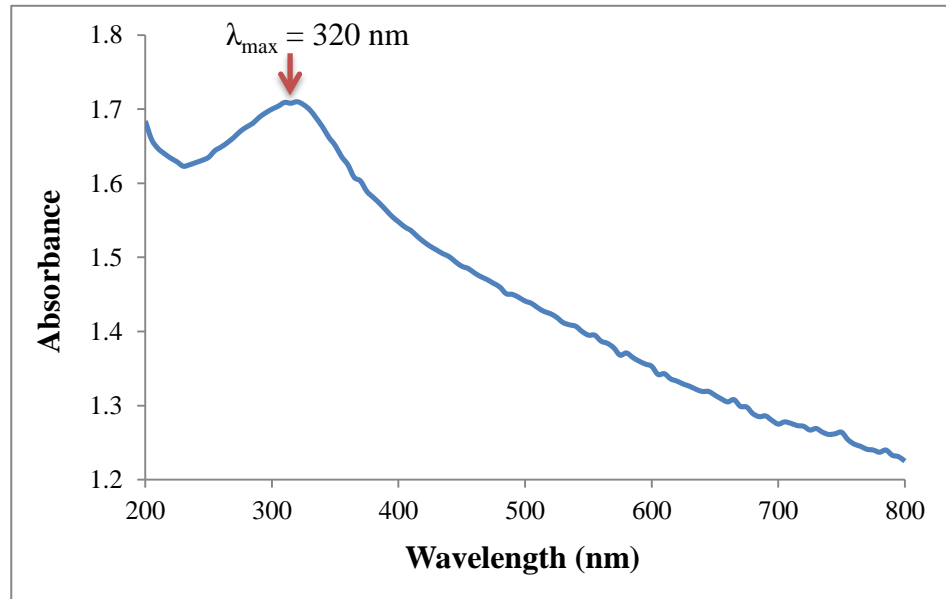


Figure 4.5 UV-Visible spectrum of synthesized NiO NPs.

As shown in Figure 4.5, the UV-Visible spectrum range from 200 – 800 nm showed that the most intense absorption peak (maximum absorbance) appeared at 320 nm. The peak was noticed at 320 nm due to the excitation of longitudinal plasmon resonance vibration and surface plasmon resonance of NiO NPs. This is the optical absorption of synthesized NiO NPs used to determine the band gap energy by using the equation (4.3) as shown below. The band gap energy is the energy difference between valence band and conduction band. Upon solar irradiation, the electrons at the valence band of synthesized semiconductor, NiO NPs excited to conduction band forming the electron-hole pairs.

$$E_{\text{bg}} = \frac{hc}{\lambda} \quad (4.3)$$

where,

h = Planck's constant ($6.63 \times 10^{-34} \text{ m}^2 \text{ kg s}^{-1}$)

c = Speed of light ($3.00 \times 10^8 \text{ m s}^{-1}$)

λ = Absorption wavelength in UV region (320 nm)

The band gap energy, E_{bg} calculated was 3.88 eV as shown in Appendix E. The value of band gap energy obtained was matched with the literature values which in the range of 3.6 – 4.0 eV.

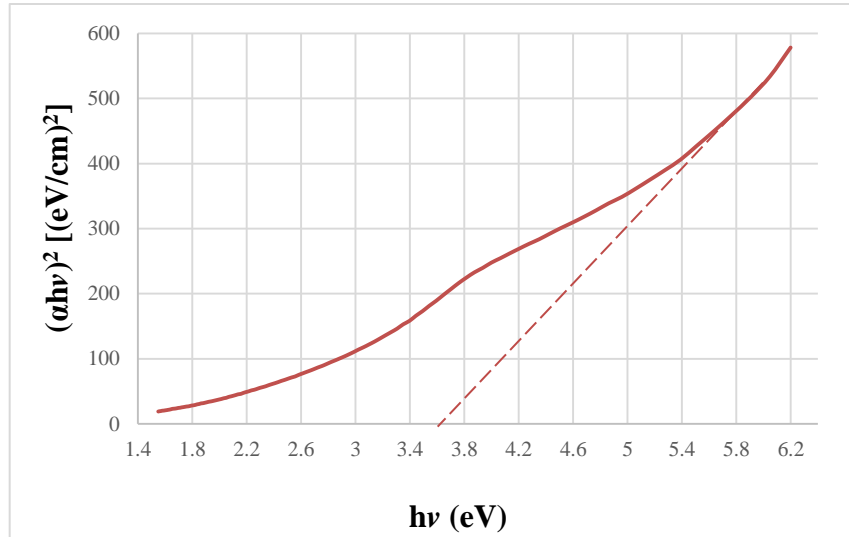


Figure 4.6 Tauc plot of synthesized NiO NPs.

The band gap energy (E_{bg}) of the synthesized NiO NPs was calculated by using Tauc relation based on the following equation (4.4):-

$$(\alpha h\nu)^{1/n} = A (h\nu - E_{bg}) \quad (4.4)$$

where α is light absorption coefficient of the material, A is a constant, h is planck's constant, ν is light frequency, E_{bg} is optical band gap of the nanoparticles and exponent n depends on the type of transition. The $n = 1/2$ is for direct allowed transition, $n = 2$ is for indirect allowed transition, $n = 3/2$ is for direct forbidden transition and $n = 3$ is for indirect forbidden transition (Mariam et al., 2014). In this study, direct allowed transition was introduced by plotting $(\alpha h\nu)^2$ against $h\nu$ as shown in Figure 4.6. The direct band gap value of synthesized NiO NPs was found to be 3.6 eV by extrapolating the linear region of the curve to $(\alpha h\nu)^2 = 0$.

The obtained band gap energy value was in agreement as it is fall within the range of the values reported in the literature which is 3.6 – 4.0 eV.

The absorption coefficient, α can be calculated by using equation (4.5) below:-

$$\alpha = \frac{2.303 \times \text{Abs}}{d} \quad (4.5)$$

where Abs is absorbance and d is path length for liquid cell / thickness for thin films.

The general relationship between the band gap energy, E_{bg} (eV) of a NiO NPs and its wavelength, λ (nm), is shown as the equation (4.6) below:-

$$\lambda = \frac{1240}{E_{bg}} \quad (4.6)$$

Therefore, this equation showed that the shorter the absorption wavelength of NiO NPs, the wider of its band gap energy (Ahmed, 2012).

4.2.5 Scanning Electron Microscopy (SEM)

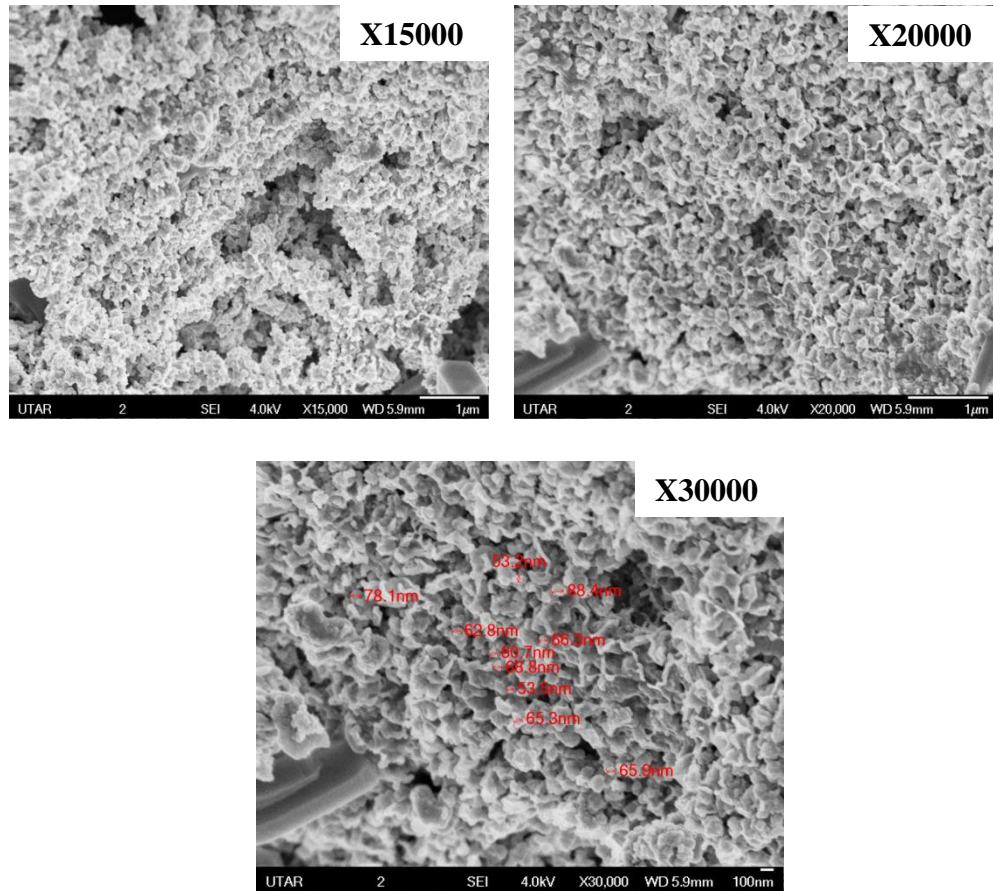


Figure 4.7 SEM images of synthesized NiO NPs at different magnifications,

X = 15000, 20000 and 30000.

SEM images as shown in Figure 4.7 revealed that the synthesized NiO NPs were spherical in shape with highly agglomeration as they are essentially a cluster of nanoparticles. The tendency of NiO NPs to agglomerate to form some larger size of nanoparticles was due to high surface tension and high surface energy of the ultrafine nanoparticles (Fardood, Ramazani and Moradi, 2017) and capping of

nanoparticles by bioactive compounds present in the papaya peel extract as confirmed from FTIR analysis (Mude et al., 2009). The agglomeration of NiO NPs may also be attributed to their polymer adherence and presence of magnetic interactions among the nanoparticles (Ezhilarasi et al., 2016). They tend to agglomerate in order to minimize the total surface energy of the system (Mariam et al., 2014). SEM images also showed that the synthesized NiO NPs were almost homogenous and uniformly distributed with uniform particle dimension (shape and size). The sizes of synthesized NiO NPs were found to be in the range of 50 – 90 nm, with an average particle size of 66.3 nm. The crystallite size of NiO NPs determined by SEM was different significantly from that obtained from XRD as the crystallite size of NiO NPs determined by XRD was the size of coherently diffracting domains within the nanoparticles (Azhagu Raj, AlSalhi and Devanesan, 2017).

4.3 Evaluation of Photocatalytic Activity of Synthesized Nickel Oxide Nanoparticles

In this study, the photocatalytic activity of synthesized NiO NPs was evaluated through the degradation of cationic dye (Methylene blue) aqueous solution under natural solar irradiation. The degradation extent of Methylene Blue (MB) dye aqueous solution was monitored by UV–Vis spectroscopy under different irradiation time. The percentage of MB dye degradation was calculated based on the absorbance values obtained to determine the photocatalytic efficiency of the synthesized NiO NPs. The occurrence of MB dye degradation can also be detected visually through the change of colour from dark blue to light blue and lastly turned into colorless solution. The percentage of dye degradation and photocatalytic efficiency were calculated and examined under three different conditions which are light condition with photocatalyst, dark condition with photocatalyst and light condition without photocatalyst.

4.3.1 Degradation of Methylene Blue (MB) Dye in Aqueous Solution Using NiO NPs under Solar Irradiation

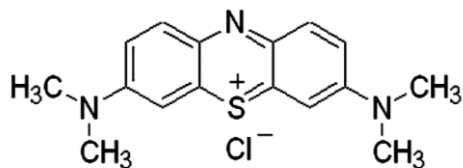


Figure 4.8 Chemical structure of MB (Chekir et al., 2015).

Methylene blue is a cationic dye with a highly conjugated system in the chemical structure. The molecular formula of MB is $C_{16}H_{18}N_3SCl$ and its IUPAC name is 3,7-bis(Dimethylamino)-phenothiazin5-ium chloride (Mohabansi, Patil and Yenkie, 2011). The chemical structural formula of MB is as shown in Figure 4.8. The physical appearance of MB is blue in color by absorbing energy from the wavelength of red region in the visible spectrum. The maximum wavelength, λ_{max} of MB is at 665 nm.

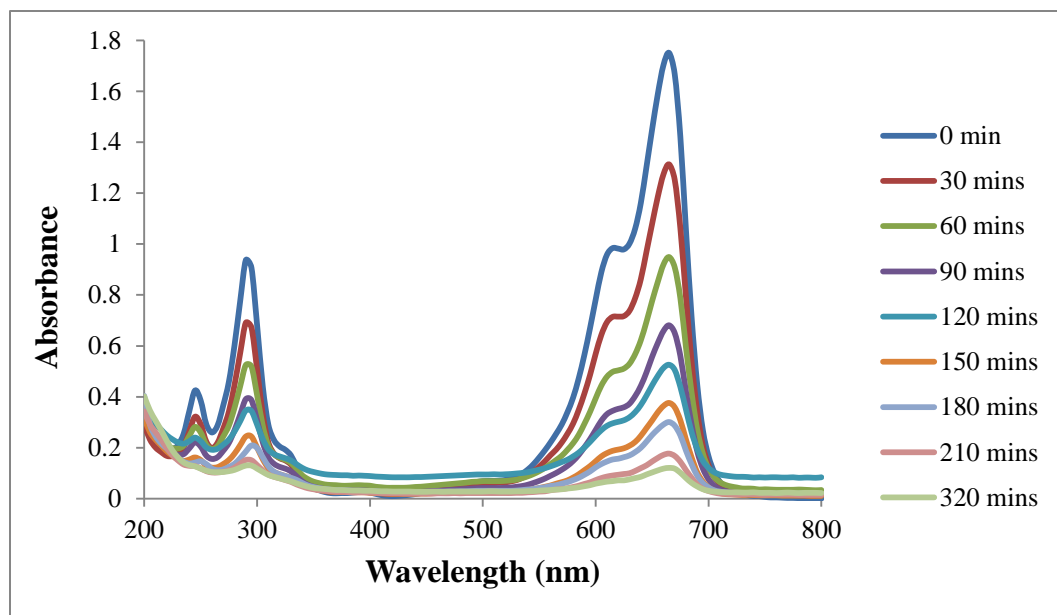


Figure 4.9 UV-Vis spectra of MB dye degradation in the presence of photocatalyst NiO NPs under solar irradiation as a function of contact time (minutes).

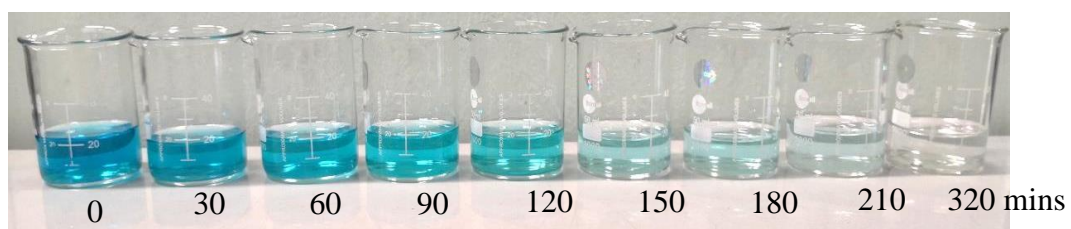


Figure 4.10 Photograph of color change of degraded MB dye aqueous solution at different time interval.

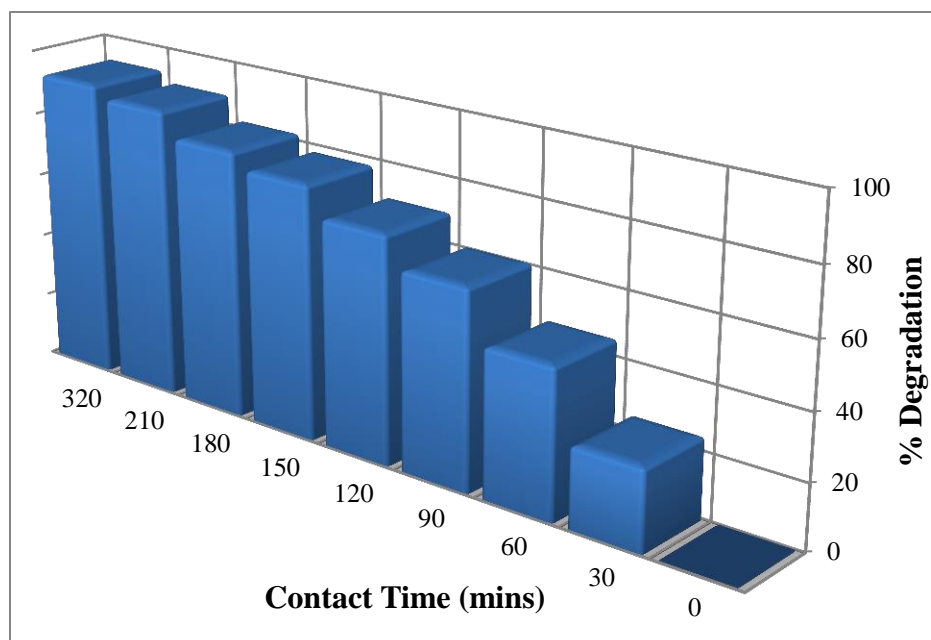


Figure 4.11 Percentage of degradation of MB dye solution as a function of time.

There are presences of two minor peaks at the wavelength of 245 nm and 290 nm respectively as shown in the UV-Vis spectra in Figure 4.9 were due to the chromophoric absorption. A 10 ppm of MB dye aqueous solution prepared was used as the control (0 minute). The absorbance of MB dye solution measured at 665 nm was 1.751. According to the UV-Vis spectra, the degradation of MB dye aqueous solution was performed within 320 minutes. It was showed that the color of the MB dye aqueous solution faded from the original dark blue color to light blue color and lastly became colorless solution after 320 minutes under solar irradiation as shown in the photograph of color change in Figure 4.10. The fading of color can be explained due to the destruction of chromophore groups in the chemical structure of MB.

From the UV-Vis spectra shown in Figure 4.9, the intensity of the absorption peak decreases with time and this indicated that the degradation of the MB dye aqueous solution increases as the reaction time increases from 0 minute to 320 minutes when exposed to solar irradiation. The higher the intensity of the absorption peak, the greater the concentration of MB dye solution as the absorbance is depend on the number of dye molecules present in the solution. The MB dye molecules were allowed to be adsorbed onto the surface active sites of NiO NPs until a saturation point was reached to allow the dye degradation process can be performed. The rate of degradation process became slower when the reaction time is longer as there are decreases in the amount of the available, free active sites of NiO NPs to let the dye molecule to adsorb on. These have been proved by the slight increases in percentage of degradation with longer contact time. The absorbance value measured at the absorption peak of 665 nm for MB dye aqueous solution show a significant decreases from 1.751 at 0 minute to 0.121 at 320 minutes. The percentage of degradation in 320 minutes contact time for MB dye aqueous solution was shown in Figure 4.11 and the overall percentage of degradation calculated was 93.09 % as shown in Appendix F. Therefore, the results obtained clearly indicated that synthesized NiO NPs able to be act as efficient and excellent photocatalyst in photodegradation process of MB dye from the aqueous medium. In this work, the exceptional photocatalytic activity of the NiO NPs was attributed to the high surface area, small particle size, photoelectron/hole separation efficiency, great electrical and optical properties, high separation rate of charge carriers and extension of the wavelength range of photoexcitation (Ahmed, 2012).

During the photodegradation process, MB dye solution undergoes a series of N-demethylation pathway in the first four steps of reaction as shown in Figure 4.12. These reactions remove the methyl group from the nitrogen atom placed in each side of the two benzene rings. The reaction is then followed by deamination for each side of the benzene ring and finally carbon dioxide and water formed as the degradation products.

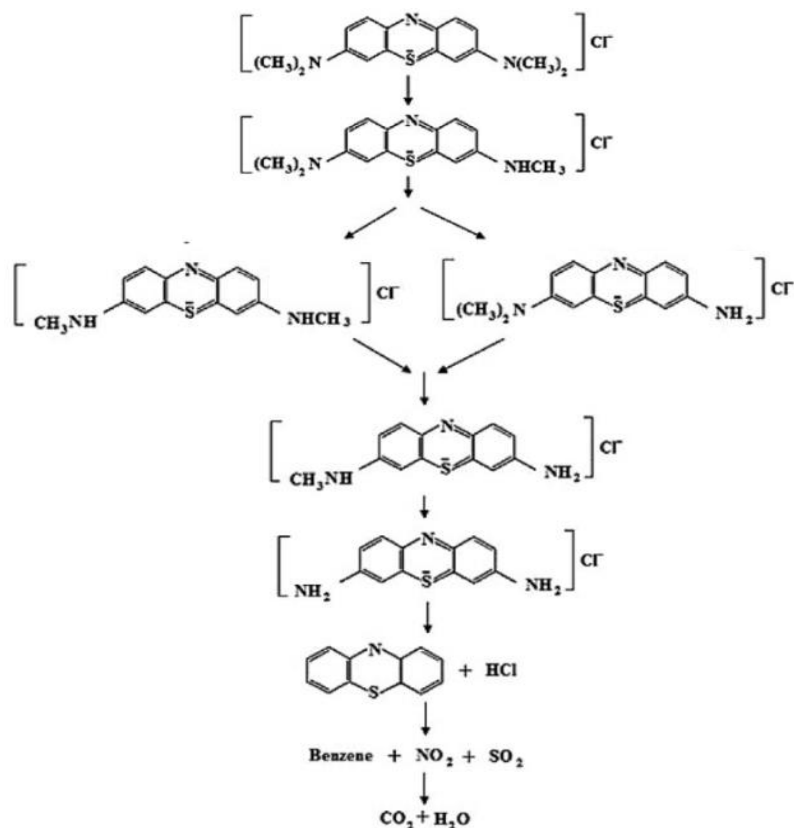


Figure 4.12 Photocatalytic reaction pathway of MB dye (Dariani et al., 2016).

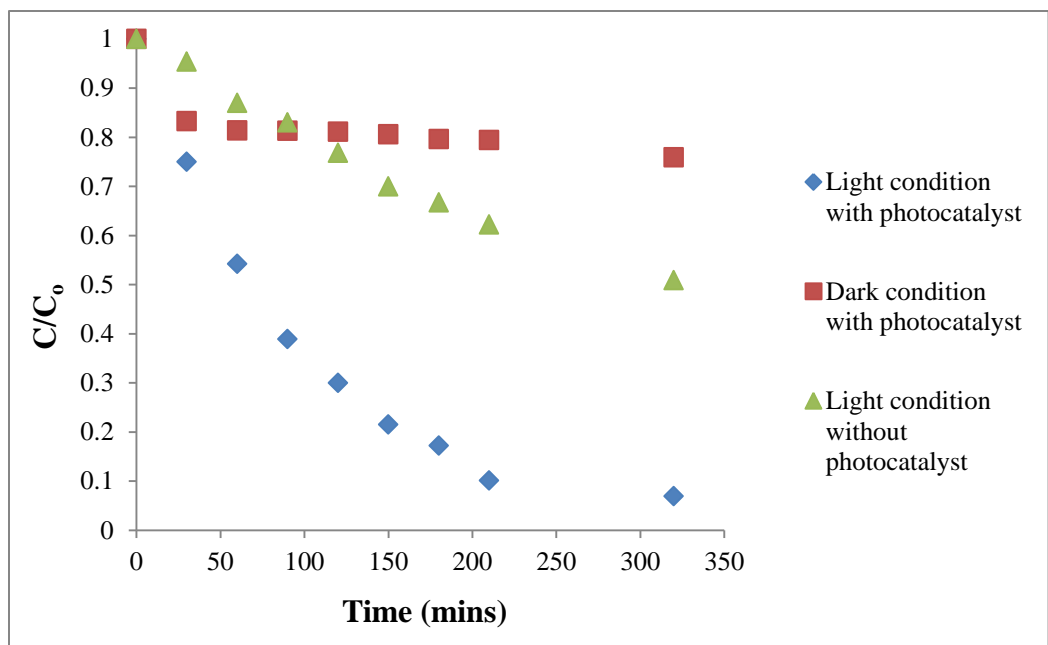


Figure 4.13 Graph of C/C_0 against time.

The graph of C/C_0 against time was shown in Figure 4.13. C/C_0 , where C_0 is the initial absorbance of MB dye solution while C is absorbance of the MB dye solution at various interval times. There are three different kinds of conditions which are light condition with photocatalyst, dark condition with photocatalyst and light condition without photocatalyst were carried out to examine the photocatalytic efficiency of synthesized NiO NPs in the photodegradation of MB dye solution. Light condition with photocatalyst was carried out by mixing 50 mg of synthesized NiO NPs with 50 mL of MB dye aqueous solution and then placed under the solar irradiation after magnetically stirred in dark for 30 minutes. Dark condition with photocatalyst was carried out by mixing 50 mg of synthesized NiO NPs with 50 mL of MB dye aqueous solution and then placed in the dark instead of exposed to sunlight after magnetically stirred in dark for 30 minutes. Light

condition without photocatalyst was carried out by placing only MB dye aqueous solution under the solar irradiation. The sample solutions were collected at a specified time interval and then proceed to the centrifugation process and lastly subjected to the UV-Vis spectroscopy in order to measure the absorbance of the sample solution collected. These three conditions were conducted according to the same time intervals. As shown in Figure 4.13, MB dye aqueous solution degraded the most in light condition with photocatalyst (93.09 %), followed by light condition without photocatalyst (43.46 %) and lastly by dark condition with photocatalyst (20.56 %) after 320 minutes. There are only slight changes of the absorbance values in the dark condition with photocatalyst due to the absence of light energy to excite the electrons of semiconductor from valence band to conduction band to generate the hydroxyl radical which react with the dye molecules to produce degradation products. The small decreases of the absorbance value in dark condition were caused by adsorption of the dye molecules on the surface active sites of the NiO NPs. However, there are drastic changes of the absorbance value in the light condition with catalyst due to the presence of light energy which is equal or greater to its band gap energy so that the excitation of electrons can be occurred and hydroxyl radical able to be generated and thus the photodegradation process of MB dye aqueous solution can be performed well. Therefore, it was concluded that the synthesized NiO NPs can act as an effective and powerful photocatalyst in the photodegradation process of MB dye aqueous solution in order to fasten up the reaction and shorten the reaction time.

CHAPTER 5

CONCLUSION

In this study, NiO NPs were successfully synthesized through green synthetic pathway by using *Carica Papaya* peel extract which act as a reducing agent and stabilizing agent in synthesis of NiO NPs. The use of papaya peel extracts for making NiO NPs is inexpensive, rapid, simple, easily scaled up, economical and environmentally benign. The synthesized NiO NPs was characterized using Ultraviolet-Visible Spectroscopy (UV-Vis), Fourier Transform Infrared Spectroscopy (FTIR), Energy Dispersive X-ray Spectroscopy (EDX), X-ray Diffraction (XRD) and Scanning Electron Microscopy (SEM).

SEM images revealed that the synthesized NiO NPs were spherical in shape with highly agglomeration and an average particle size of 66.3 nm. The average crystallite size of synthesized NiO NPs calculated by using Debye-Scherrer equation was 13.39 nm according to the FWHM of highest intense peak of XRD pattern and XRD pattern also indicated that the synthesized NiO NPs having face centered cubic phase. From the FTIR analysis, the Ni-O stretching vibration mode appeared at absorption band of 458 cm^{-1} which further confirmed the formation of NiO NPs. The UV-Vis peak was observed for NiO NPs at 320 nm. The band gap energy, E_{bg} of synthesized NiO NPs calculated was 3.88 eV while the direct band

gap value of synthesized NiO NPs determined from Tauc plot was found to be 3.6 eV.

According to the photocatalytic degradation study, the photocatalytic activity of synthesized NiO NPs was evaluated through the degradation of MB dye aqueous solution under natural solar irradiation. The results obtained showed that the synthesized NiO NPs are an effective and excellent photocatalyst used in the photodegradation process of MB dye as 93.09 % of MB dye aqueous solutions was successfully degraded within 320 minutes.

In order to further study in this project, the photodegradation process of MB dye aqueous solution can be analyzed by using Liquid Chromatography-Mass Spectrometry (LC-MS) and Gas Chromatography-Mass Spectrometry (GC-MS) to determine intermediate degradation products formed during MB dye degradation. Furthermore, a tentative mechanism of possible degradation pathway for MB dye aqueous solution can also be proposed, identified and analyzed by using LC-MS and GC-MS.

REFERENCES

Journal:

Ahmed, M. (2012). Synthesis and structural features of mesoporous NiO/TiO₂ nanocomposites prepared by sol–gel method for photodegradation of methylene blue dye. *Journal of Photochemistry and Photobiology A: Chemistry*, 238, pp.63-70.

Ahmed, S. and Ikram, S. (2015). Synthesis of Gold Nanoparticles using Plant Extract: An Overview. *Nano Research & Applications*, 1(1:5), pp.1-6.

Ajoudanian, N. and Nezamzadeh-Ejhieh, A. (2015). Enhanced photocatalytic activity of nickel oxide supported on clinoptilolite nanoparticles for the photodegradation of aqueous cephalixin. *Materials Science in Semiconductor Processing*, 36, pp.162-169.

Akhtar, M., Panwar, J. and Yun, Y. (2013). Biogenic Synthesis of Metallic Nanoparticles by Plant Extracts. *ACS Sustainable Chemistry & Engineering*, 1(6), pp.591-602.

Azhagu Raj, R., AlSalhi, M. and Devanesan, S. (2017). Microwave-Assisted Synthesis of Nickel Oxide Nanoparticles Using *Coriandrum sativum* Leaf Extract and Their Structural-Magnetic Catalytic Properties. *Materials*, 10(5), p.460.

Chakraborty, A., Roy, T. and Mondal, S. (2016). Development of DNA Nanotechnology and Uses in Molecular Medicine and Biology. *Insights in Biomedicine*, 1(2:13), pp.1-10.

Chekir, N., Benhabiles, O., Tassalit, D., Laoufi, N. and Bentahar, F. (2015). Photocatalytic degradation of methylene blue in aqueous suspensions using TiO₂ and ZnO. *Desalination and Water Treatment*, 57(13), pp.6141-6147.

Dariani, R., Esmaeili, A., Mortezaali, A. and Dehghanpour, S. (2016). Photocatalytic reaction and degradation of methylene blue on TiO₂ nano-sized particles. *Optik*, 127(18), pp.7143-7154.

Donda, M., Kudle, K., Alwala, J., Miryala, A., Sreedhar, B. and Rudra, M. (2013). Synthesis of silver nanoparticles using extracts of *Securinega leucopyrus* and evaluation of its antibacterial activity. *International Journal of Current Science*, 7, pp.1-8.

El-Debaiky, S., El-Badry, A. and El-Shahawy, M. (2017). Biosynthesis of Nickel Oxide Nanoparticles Using *Fusarium verticillioides* (Sacc.) and Their Biological Activity against Some Causative Agents of Mycotic Keratitis. *Egyptian Journal of Botany*, 57(3), pp.417- 428.

Ezhilarasi, A., Vijaya, J., Kaviyarasu, K., Maaza, M., Ayeshamariam, A. and Kennedy, L. (2016). Green synthesis of NiO nanoparticles using *Moringa oleifera* extract and their biomedical applications: Cytotoxicity effect of nanoparticles against HT-29 cancer cells. *Journal of Photochemistry & Photobiology, B: Biology*, 164, pp.352-360.

Fardood, S., Ramazani, A. and Moradi, S. (2017). A Novel Green Synthesis of Nickel Oxide Nanoparticles Using Arabic Gum. *Chemistry Journal of Moldova*, 12(1), pp.115-118.

Haleemkhan, A., Naseem and Vardhini, B. (2015). Synthesis of Nanoparticles from Plant Extracts. *International Journal of Modern Chemistry and Applied Science*, 2(3), pp.195-203.

Helan, V., Prince, J., Al-Dhabi, N., Arasu, M., Ayeshamariam, A., Madhumitha, G., Roopan, S. and Jayachandran, M. (2016). Neem leaves mediated preparation of NiO nanoparticles and its magnetization, coercivity and antibacterial analysis. *Results in Physics*, 6, pp.712-718.

Imran Din, M. and Rani, A. (2016). Recent Advances in the Synthesis and Stabilization of Nickel and Nickel Oxide Nanoparticles: A Green Adeptness. *International Journal of Analytical Chemistry*, 2016, pp.1-14.

Jain, D., Daima, H., Kachhwaha, S. and Kothari, S. (2009). Synthesis of Plant-Mediated Silver Nanoparticles using Papaya Fruit Extract and Evaluation of Their Anti Microbial Activities. *Digest Journal of Nanomaterials and Biostructures*, 4(3), pp.557 - 563.

Jain, S. and Mehata, M. (2017). Medicinal Plant Leaf Extract and Pure Flavonoid Mediated Green Synthesis of Silver Nanoparticles and their Enhanced Antibacterial Property. *Scientific Reports*, 7(1), pp.1-13.

Mariam, A., Kashif, M., Arokiyaraj, S., Bououdina, M., Sankaracharyulu, M., Jayachandran, M. and Hashim, U. (2014). Bio-Synthesis of NiO and Ni Nanoparticles and Their Characterization. *Digest Journal of Nanomaterials and Biostructures*, 9(3), pp.1007 - 1019.

Mittal, A., Chisti, Y. and Banerjee, U. (2013). Synthesis of metallic nanoparticles using plant extracts. *Biotechnology Advances*, 31(2), pp.346-356.

Mohabansi, N., Patil, V. and Yenkie, N. (2011). A Comparative Study on Photo Degradation of Methylene Blue Dye Effluent by Advanced Oxidation Process by using TiO₂/ZnO Photo Catalyst. *Rasayan Journal of Chemistry*, 4(4), pp.814-819.

Mude, N., Ingle, A., Gade, A. and Rai, M. (2009). Synthesis of Silver Nanoparticles Using Callus Extract of *Carica papaya* — A First Report. *Journal of Plant Biochemistry and Biotechnology*, 18(1), pp.83-86.

Nasseri, M., Ahrari, F. and Zakerinasab, B. (2016). A green biosynthesis of NiO nanoparticles using aqueous extract of *Tamarix serotina* and their characterization and application. *Applied Organometallic Chemistry*, 30(12), pp.978-984.

Pareek, V., Bhargava, A., Gupta, R., Jain, N. and Panwar, J. (2017). Synthesis and Applications of Noble Metal Nanoparticles: A Review. *Advanced Science, Engineering and Medicine*, 9(7), pp.527–544.

Qing, Z., Haixia, L., Huali, L., Yu, L., Huayong, Z. and Tianduo, L. (2015). Solvothermal synthesis and photocatalytic properties of NiO ultrathin nanosheets with porous structure. *Applied Surface Science*, 328, pp.525-530.

Sharma, J., Srivastava, P., Singh, G., Akhtar, M. and Ameen, S. (2015). Biosynthesized NiO nanoparticles: Potential catalyst for ammonium perchlorate and composite solid propellants. *Ceramics International*, 41(1), pp.1573-1578.

Soofivand, F. and Salavati-Niasari, M. (2017). Step synthesis and photocatalytic activity of NiO/graphene nanocomposite under UV and visible light as an effective photocatalyst. *Journal of Photochemistry and Photobiology A: Chemistry*, 337, pp.44-53.

Thema, F., Manikandan, E., Gurib-Fakim, A. and Maaza, M. (2016). Single phase Bunsenite NiO nanoparticles green synthesis by *Agathosma betulina* natural extract. *Journal of Alloys and Compounds*, 657, pp.655-661.

APPENDICES

Appendix A

Crystalline size of synthesized NiO NPs

Calculation for β

$$\begin{aligned}\beta &= \frac{\text{FWHM in } 2\theta \times \pi}{180^\circ} \\ &= \frac{0.81680^\circ \times \pi}{180^\circ} \\ &= 0.01426\end{aligned}$$

Calculation for crystalline size by Debye-Scherrer Equation

$$\begin{aligned}D &= \frac{k\lambda}{\beta \cos\theta} \\ &= \frac{0.9 \times (1.5406 \times 10^{-10} \text{ m})}{(0.01426) \cos 43.4504} \\ &= 13.39 \text{ nm}\end{aligned}$$

where,

D = Average crystalline diameter size

k = Scherrer constant (usually 0.9)

λ = Wavelength of X-ray source, (Cu K α radiation = 1.5406 Å)

β = Full width at half-maximum (FWHM) of the X-ray diffraction peak in radian

2θ

θ = Bragg's diffraction angle

Appendix B

```
*** Basic Data Process ***

# Data Information
  Group           : Standard
  Data            : KHW_NiONPS1812
  Sample Name     : NiONPS1812
  Comment         : NiONPS1812
  Date & Time     : 03-20-18 13:51:21

# Measurement Condition
  X-ray tube
    target        : Cu
    voltage       : 40.0 (kV)
    current       : 30.0 (mA)
  Slits
    Auto Slit     : not Used
    divergence slit : 1.00000 (deg)
    scatter slit  : 1.00000 (deg)
    receiving slit : 0.30000 (mm)
  Scanning
    drive axis    : Theta-2Theta
    scan range    : 10.0000 - 80.0000 (deg)
    scan mode     : Continuous Scan
    scan speed    : 2.0000 (deg/min)
    sampling pitch : 0.0200 (deg)
    preset time   : 0.60 (sec)

# Data Process Condition
  Smoothing       [ AUTO ]
    smoothing points : 49
  B.G.Subtraction [ AUTO ]
    sampling points  : 51
    repeat times     : 30
  Kal-a2 Separate [ MANUAL ]
    Kal a2 ratio     : 50 (%)
  Peak Search     [ AUTO ]
    differential points : 41
    FWHM threshold    : 0.050 (deg)
    intensity threshold : 30 (par mil)
    FWHM ratio (n-1)/n : 2
  System error Correction [ NO ]
  Precise peak Correction [ NO ]
```

Figure: Information for XRD analysis (I)

Appendix C

```

*** Basic Data Process ***

Group      : Standard
Data       : KHW_NiONPS1812

# Strongest 3 peaks
no. peak   2Theta      d      I/I1    FWHM      Intensity  Integrated Int
no.        (deg)        (Å)    (deg)    (Counts)  (Counts)
  1  26    43.4504    2.08102  100    0.81680    2127    96681
  2  22    37.3781    2.40394   50    0.89830    1066    49496
  3  31    63.1124    1.47191   42    0.98280     887    51632

# Peak Data List
peak       2Theta      d      I/I1    FWHM      Intensity  Integrated Int
no.        (deg)        (Å)    (deg)    (Counts)  (Counts)
  1    14.0400    6.30279    4    1.04000     87     5688
  2    14.6600    6.03759    6    0.82800    132     5951
  3    15.6400    5.66141    4    0.00000     90        0
  4    16.5600    5.34891    4    0.00000     86        0
  5    17.4800    5.06940    4    0.00000     88        0
  6    18.0000    4.92411    4    0.00000     90        0
  7    19.1600    4.62852    4    0.00000     86        0
  8    20.3400    4.36259    5    0.00000     99        0
  9    21.3130    4.16557   10    0.75940    219    11568
 10    22.2000    4.00110    3    0.00000     70        0
 11    23.7400    3.74492    4    0.98000     90     7685
 12    25.5616    3.48203    5    0.61670    105     3145
 13    26.6985    3.33628    4    1.20290     85     4425
 14    27.6000    3.22932    4    0.39420     80     2075
 15    28.3911    3.14111   27    0.61320    577    18431
 16    29.7268    3.00294   29    0.72720    619    24861
 17    30.9297    2.88884   37    0.73850    784    27026
 18    31.6400    2.82559   12    0.52720    245     9265
 19    32.4200    2.75936    4    0.00000     79        0
 20    33.6912    2.65810    8    0.80250    178    10395
 21    36.0200    2.49140    7    0.89600    154    10037
 22    37.3781    2.40394   50    0.89830   1066    49496
 23    39.0800    2.30308    9    0.70340    184     8513
 24    40.5594    2.22243   14    0.59310    292     8957
 25    42.1200    2.14362    4    0.56000     91     6437
 26    43.4504    2.08102  100    0.81680   2127    96681
 27    45.2800    2.00109    3    0.47200     68     5104
 28    50.2366    1.81465    4    0.56670     84     4012
 29    56.4570    1.62858    5    0.92600    109     8399
 30    58.6719    1.57227    3    0.53040     65     2434
 31    63.1124    1.47191   42    0.98280    887    51632
 32    64.9800    1.43404    5    1.01600    114     8440
 33    66.4400    1.40603    4    0.62000     83     4596
 34    75.6460    1.25615   12    1.16400    261    19105
 35    79.8400    1.20037    9    1.24000    191     9206

```

Figure: Information for XRD analysis (II)

Appendix D

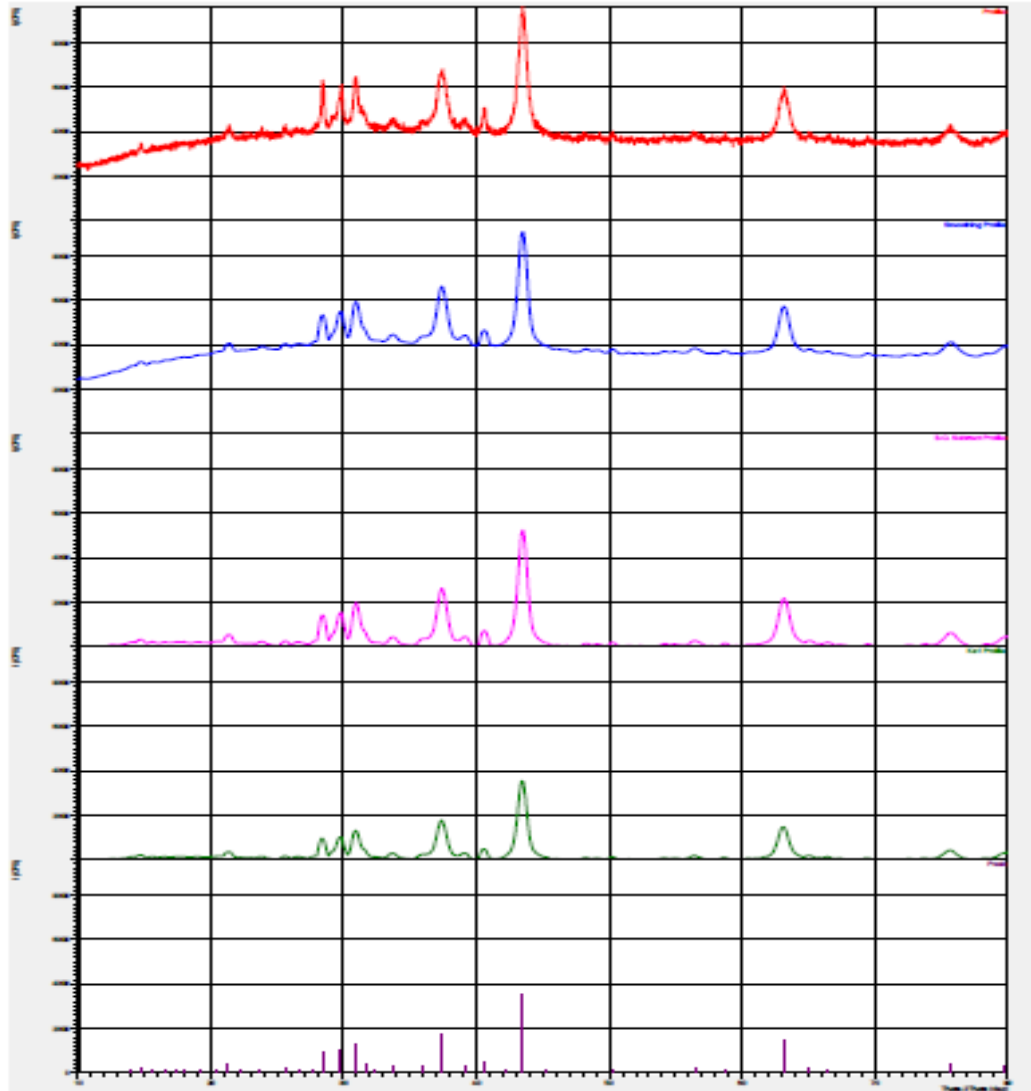


Figure: Information for XRD analysis (III)

Appendix E

Calculation for band gap energy, E_{bg}

$$\begin{aligned} E_{bg} &= \frac{hc}{\lambda} \\ &= \frac{(6.63 \times 10^{-34} \text{ m}^2 \text{ kg s}^{-1}) \times (3.00 \times 10^8 \text{ m s}^{-1})}{320 \text{ nm}} \\ &= 6.63 \times 10^{-19} \times 6.242 \times 10^{18} \text{ eV} \\ &= 3.88 \text{ eV} \end{aligned}$$

where,

h = Planck's constant ($6.63 \times 10^{-34} \text{ m}^2 \text{ kg s}^{-1}$)

c = Speed of light ($3.00 \times 10^8 \text{ m s}^{-1}$)

λ = Absorption wavelength in UV region (320 nm)

Appendix F

$$\text{Percentage of Dye Degradation} = \frac{A_o - A_t}{A_o} \times 100\%$$

where,

A_o = Initial absorbance of dye solution before expose to sunlight

A_t = Absorbance of dye solution after photocatalytic degradation at different irradiation time (t)

Effects of Contact Time in Degradation of MB dye by NiO NPs

Table: Degradation Percentage of MB dye as a function of contact time

Contact Time (mins)	Initial Absorbance	Final Absorbance	Degradation Percentage (%)
0	1.751	1.751	0
30	1.751	1.313	25.01
60	1.751	0.949	45.80
90	1.751	0.681	61.11
120	1.751	0.526	69.96
150	1.751	0.376	78.53
180	1.751	0.301	82.81
210	1.751	0.177	89.89
320	1.751	0.121	93.09